

Original paper

# SIMS U–Pb zircon dating and Re–Os isotopic analysis of the Hulu Cu–Ni deposit, eastern Tianshan, Central Asian Orogenic Belt, and its geological significance

Chunming HAN<sup>1</sup>, Wenjiao XIAO<sup>2,1\*</sup>, Guochun ZHAO<sup>3</sup>, Ben-Xun SU<sup>1,3</sup>, Patrick Asamoah SAKYI<sup>4</sup>, Songjian AO<sup>1</sup>, Bo WAN<sup>1</sup>, Ji'en ZHANG<sup>1</sup>, Zhiyong ZHANG<sup>1</sup>

<sup>1</sup> Institute of Geology and Geophysics, Chinese Academy of Sciences, Beijing 100029, China; wj-xiao@mail.iggcas.ac.cn

<sup>2</sup> Xinjiang Research Center for Mineral Resources, Xinjiang Institute of Ecology and Geography, Chinese Academy of Sciences, Urumqi 830011, China

<sup>3</sup> Department of Earth Sciences, The University of Hong Kong, Pokfulam Road, Hong Kong, China

<sup>4</sup> Department of Earth Science, University of Ghana, P.O. Box LG 58, Legon-Accra, Ghana

\* Corresponding author



Exploration of the Hulu Cu–Ni–Co sulfide deposit in Eastern Tianshan, Central Asian Orogenic Belt, has detected horizons of sulfide mineralization in pyroxenite and peridotite units. SIMS U–Pb zircon ages of the gabbro-hosting Cu–Ni–Co sulfide deposit indicate that the Hulu intrusion was emplaced at  $282.3 \pm 1.2$  Ma (95% confidence level, MSWD = 3.30,  $n = 13$ ). Osmium isotopic data suggest that the Hulu intrusion and associated Cu–Ni mineralization were derived from crustally-contaminated mantle melts. The intrusions clearly show island-arc geochemical signatures, such as negative Nb, Ta, Zr and Ti anomalies and enrichment in LILE. These geochemical tracers indicate that the Hulu mafic–ultramafic intrusions, along with the Cu–Ni deposit, formed as a result of subduction of oceanic crust in the Early Permian. The arc-related geodynamic setting of the Hulu Cu–Ni deposit is unusual for magmatic sulfide deposits. This new type of ore deposit offers an alternative perspective for Cu and Ni exploration.

**Keywords:** Hulu Complex, SIMS U–Pb zircon, Re–Os isotopic data, Cu–Ni deposit, Eastern Tianshan, Central Asian Orogenic Belt

**Received:** 16 March 2013; **accepted:** 11 September 2013; **handling editor:** E. Jelínek

## 1. Introduction

In northern Xinjiang, sixteen Uralian–Alaskan-type mafic–ultramafic complexes are distributed in the western Tianshan (e.g. Jingbulake), eastern Junggar (e.g. Kalatongke) and eastern Tianshan (e.g. Hulu) areas (Figs

1–2). Since the discovery of the Huangshandong orebody in 1979, intense exploration and extensive geological investigations have led to the recognition of the eastern Tianshan nickel–copper belt (Mao et al. 2002; Zhou et al. 2004; Han et al. 2010). This belt ranks as the second largest Cu–Ni-producing area in Xinjiang, with Kalatongke

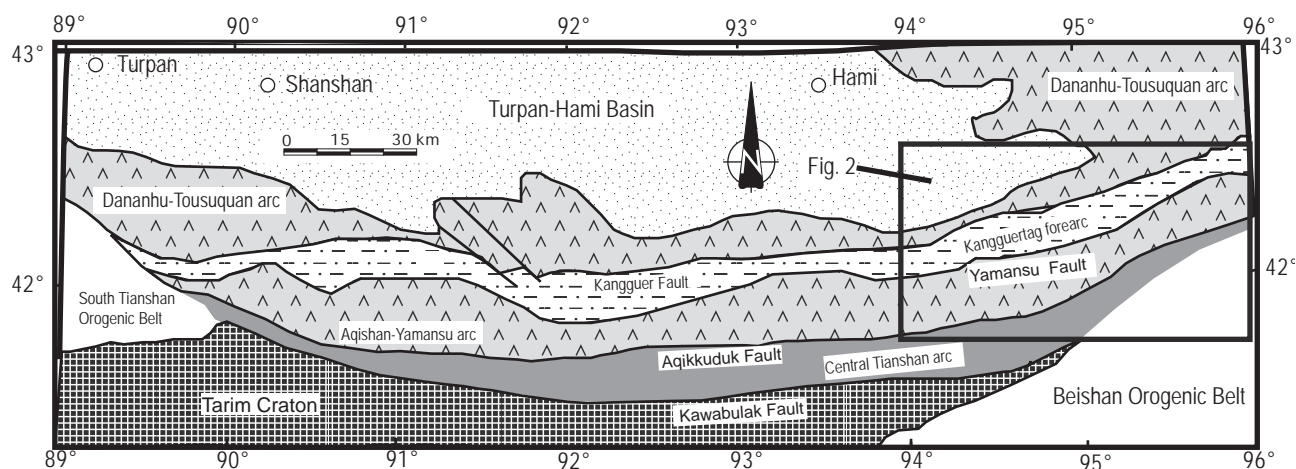


**Fig. 1** Simplified geological map of the eastern Tianshan, NW China (modified from Xiao et al. 2004b).

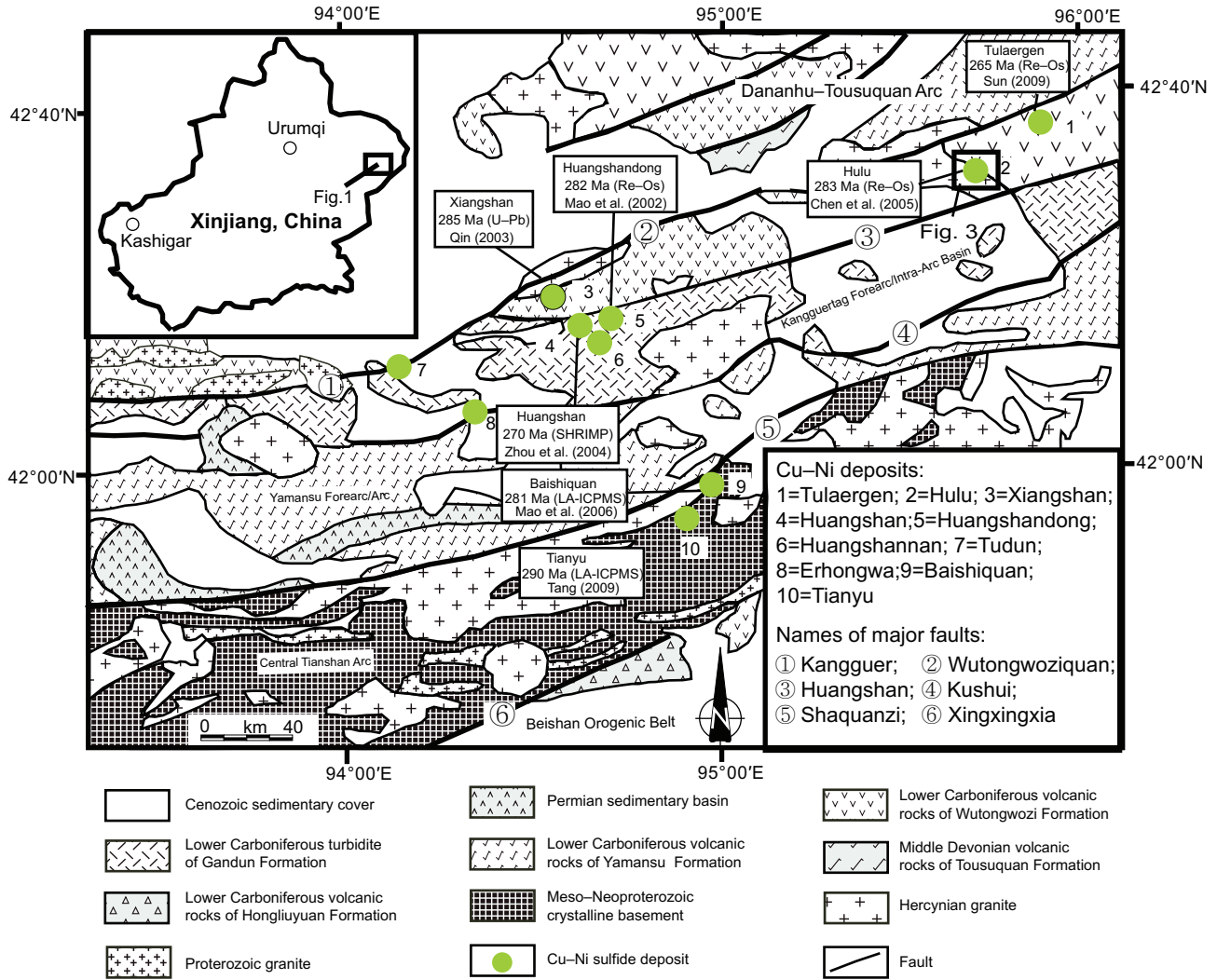


Fig. 2 Distribution of Cu-Ni deposits in the eastern Tianshan (modified from Wang et al. 2006).

as the largest deposit. To date, three mines have been in production (Tab. 1), and there are numerous other potential deposits along the belt (Han et al. 2010).

However, one of the most challenging and controversial aspects of the deposits has been the ages of the ultramafic bodies and associated nickel-copper sulfide mineralization. Over the years numerous attempts have been made by direct and indirect methods (Wang and Li 1987; Mao et al. 2002; Zhou et al. 2004; Chen et al. 2005; Han et al. 2010). Still, reliable determinations of the intrusive ages are lacking.

This paper presents the results of a SIMS U-Pb zircon study and Re-Os isotope investigations conducted on a mineralized ultramafic body from the Hulu area in the northern part of the belt. These new data provide important insights into understanding the timing and genesis of mineralization and geodynamic environment of the Hulu Cu-Ni sulfide deposit. In addition, we have attempted to constrain the provenance and geodynamic

environment of the eastern Tianshan copper-nickel belt. An understanding of these mineralizing processes and the geodynamic environment has important implications for Cu-Ni exploration potential of other mafic-ultramafic bodies in the region as well as throughout much of the Central Asian Orogenic Belt.

## 2. Regional setting

The Eastern Tianshan Orogenic Belt, the southern part of the Central Asian Orogenic Belt or Altaiids, contains a number of Paleozoic terranes, which accreted between the southern Siberian accretionary system and the Tarim Craton, and underwent a complex tectonic evolution (Coleman 1989; Xiao et al. 2004a, b; Wilhem et al. 2012; Xu et al. 2013; Zheng et al. 2013).

The Eastern Tianshan Orogenic Belt consists mainly of four tectonic units: Dananhu-Tousuquan arc,

Tab. 1 Summary of major copper–nickel deposits in the Eastern Tianshan orogenic belt

Deposit	GPS <sup>a</sup>	Status	Metals	Length × width (km)	Area (km <sup>2</sup> )	Shape	Resource and grade	Mafic–ultramafic rock types	Ore minerals
Huangshandong	95°45'00"E, 42°17'00"N	Current producer	Cu–Ni–Co–Au–Ag–PGE	5.3×1.12	2.8	Rhombus lenticle	Cu 0.1882 Mt, 0.27 %; Ni 0.3836 Mt, 0.52 %; Co 16700 t, 0.024 %	hornblende–olivine gabbro, pyroxene–hornblende gabbro, gabbro–diorite, gabbronorite, olivine gabbro–norite, pyroxene cortlandite	pyrrhotite, pentlandite, pyrite, chalcopyrite
Huangshan	94°37'00"E, 42°15'00"N	Current producer	Cu–Ni–Co–Au–Ag–PGE	3.8×8	1.71	Comet shape	Cu 0.2083 Mt, 0.31 %; Ni 0.334 Mt, 0.47 %; Co 19500 t, 0.026 %	hornblende gabbro, gabbro–diorite, hornblende gabbro–norite, hornblende lherzolite, hornblende websterite	pyrrhotite, pentlandite, violarite, cubanite, chalcopyrite
Xiangshan	94°33'18"E, 42°18'17"N	Current producer	Cu–Ni–Co–PGE	10×3.5	2.8	Lotus root	Cu 20000 t, 0.30 %; Ni 40000 t, 0.50 %	cortlandite, peridotite, pyroxene diorite, hornblende gabbro	pyrrhotite, pentlandite, violarite, cubanite, chalcopyrite
Huangshannan	94°40'00"E, 42°11'30"N	Resource	Cu–Ni	5.2×1.3	4.22	Lenticle	Cu 1300 t, 0.30 %; Ni 10000 t, 0.40 %	pyroxene–cortlandite, hornblende–pyroxenite, lherzolite, peridotite, hornblende–gabbro, norite	pyrrhotite, pentlandite, chalcopyrite, violarite, cubanite
Erhongwa	94°17'00"E, 42°07'30"N	Resource	Cu–Ni	3.33×2.56	6.25	Irregular round	Cu 4000 t, 0.20 %; Ni 18000 t, 0.20 %	lherzolite, gabbro–norite, olivine gabbro, pyroxene diorite, quartz diorite	pyrrhotite, pentlandite, pyrite, chalcopyrite
Tudun	94°10'00"E, 42°13'15"N	Resource	Cu–Ni	1.4×0.7	0.90	Irregular ellipse	Cu 3000 t, 0.20 %; Ni 15000 t, 0.30 %	gabbro, pyroxene–hornblende peridotite, pyrolite, olivine–hornblende pyroxenite	pyrrhotite, pentlandite, violarite, cubanite, chalcopyrite
Hulu	95°41'48"E, 42°31'18"N	Current producer	Cu–Ni–Co–Au–Ag–PGE	1.4×0.72	0.75	Lenticle	Cu 39600 t, 0.10–0.49 %; Ni 80200 t, 0.23–0.61 %; Co 5100 t, 0.02–0.042 %	pyrrhotite–peridotite–pyroxenite	pyrrhotite, pentlandite, millerite, violarite, chalcopyrite
Baishiquan	94°55'00"E, 41°55'00"N	Resource	Cu–Ni–PGE	1.4×0.72	0.75	Lenticle	Cu 39600 t, 0.22–0.43 %; 0.2–0.57% Ni; 0.01–0.03 % Co	troctolite–peridotite, olivine pyroxenite	pyrrhotite, pentlandite, millerite, violarite, chalcopyrite

Data mainly from Qin et al. (2003); <sup>a</sup>Longitude and latitude of the deposit

Kangguertag forearc accretionary complex, Yamansu forearc–arc and central Tianshan arc (Figs 1–2; Xiao et al. 2004b).

The *Dananhu–Tousuquan arc* is composed of Ordovician to Devonian–Carboniferous volcanic and pyroclastic rocks. The formations consist mainly of tholeiitic basalt lavas, pyroclastic rocks, clastic sediments, and calc-alkaline felsic lavas with tuffs; the Carboniferous formations consist predominantly of lavas, pyroclastic rocks, graywackes and carbonates (Yang et al. 1996, 2000; Zhou et al. 2001; Xiao et al. 2004b).

The *Kangguertag forearc* accretionary complex contains submarine lavas and pyroclastic rocks that were thrust southward over the Yamansu forearc and arc (Xiao et al. 2004b). The coherent strata include mainly Early–Middle Carboniferous volcano-sedimentary rock. The tholeiitic chemistry of volcanites in these formations suggests a forearc origin (Yang et al. 1996).

The *Yamansu forearc–arc* is characterized by volcanic rocks and terrigenous clastic sediments interbedded with limestones (Xiao et al. 2004b). Devonian basalts–andesites are imbricated with slightly metamorphosed fine-grained clastics and carbonate, and overlain by Carboniferous basalts–rhyolites, with spilite and keratophyre. The Upper Carboniferous andesite and rhyolite are interbedded with clastic sediments and limestone. The andesite is calc-alkaline, whereas the basalt corresponds to an oceanic tholeiite (Ji et al. 2000). These arc rocks contain considerable Au and volcanogenic-hosted massive sulfide (VHMS) Cu–Fe mineralization. Lower Carboniferous strata are subdivided upwards into: 1) the thick limestone and mylonitic carbonate, 2) the intermediate and felsic volcanics with pyroclastics, and 3) the limestone, clastic sediments, spilite, keratophyre and pyroclastics (Xiao et al. 2004b).

The *Central Tianshan arc* system is located between the Aqikkuduk Fault to the north and the Kawabulak Fault to the south (Xiao et al. 2004b). This unit has been regarded as a composite volcanic arc, composed of calc-alkaline basaltic andesite, volcanoclastics, minor I-type granite and granodiorite, and amphibolite-facies Precambrian basement rocks (Ma et al. 2012a, b), extends along the northern margin of the Central Tianshan arc (Fig. 1). The Precambrian basement of this arc consists of gneiss, quartz schist, migmatite, and marble (Ma et al. 2013a, b). A volcano-sedimentary assemblage was identified including Ordovician basalt–rhyolite, greywacke and the Silurian turbidite (Shu et al. 2002). Early Silurian and Early Carboniferous active margin sequences are widely exposed in the Central Tianshan magmatic arcs (Zhou et al. 2001). Silurian terrestrial clastic rocks and limestones are succeeded by Devonian limestones and terrestrial clastic rocks, overlain by Early Carboniferous volcanic rocks. They are imbricated with

deformed volcanics, clastics, limestones and ultramafic rocks (Xiao et al. 2004b).

### 3. Petrography of the Hulu intrusion

The Hulu intrusion is *c.* 1.94 km long and up to 0.72 km wide (Fig. 3). It intruded the Lower Carboniferous Wutongwozi Fm., which consists predominantly of basalt, felsite, spilite, quartz keratophyre, vitric tuff and quartzite. The Hulu intrusion contains peridotite, pyroxenite, olivine clinopyroxenite and gabbro–diorite.

The peridotite consists of (vol. %) olivine (30–90), plagioclase (1–25), hornblende (2–25), biotite (0–15), and clinopyroxene (0–20) plus sulfide minerals. It can be divided into harzburgite and lherzolite, based on the orthopyroxene and clinopyroxene contents. Most samples are highly serpentinized and exhibit a characteristic network texture in which magnetite was released along grain boundaries and cracks (Fig. 4). Irregular remnant olivine kernels typically occur in a network of serpentine minerals. Olivine is usually rounded and enclosed by orthopyroxene or clinopyroxene oikocrysts. Pyroxene and plagioclase are enclosed in hornblende. Olivine crystals have reaction rims formed by orthopyroxene.

The pyroxenite generally contains (vol. %) clinopyroxene (50–95), olivine (3–8), plagioclase (3–25), and hornblende (2–25). Most pyroxene grains were replaced by magnesium hornblende and chlorite. Clinopyroxene crystals range from 1 to 5 mm in size, and are mostly altered to serpentine along their margins. Irregular remnant olivine kernels occur in a network of serpentine minerals. Olivine is usually rounded and incorporated by orthopyroxene or clinopyroxene oikocrysts. Pyroxene and plagioclase are enclosed by hornblende. Olivine crystals have reaction rims of orthopyroxene. Intercumulus minerals include hornblende, biotite, ilmenite and trace sulfides.

The olivine clinopyroxenite consists of (vol. %) clinopyroxene (50–55), olivine (5–25), plagioclase (10–25) and hornblende (15–20); partly altered hornblende occurs with minor sulfide and chromite. Most pyroxenes have been replaced by magnesium hornblende and chlorite. Olivine crystals range from 1 to 1.5 mm in size, and are usually altered to serpentine along their margins, and they are surrounded by orthopyroxene. Clinopyroxene crystals are from 2 to 4 mm across. Greenish brown hornblende occurs as epitaxial overgrowths on orthopyroxene and olivine; alteration products include serpentine and chlorite.

The gabbro–diorite ranges from 2 to 96 m in width and amounts to about 9 % of the complex. The rock is usually gray-green, massive and medium- to coarse-grained (1–8 mm). It consists of (vol. %) pyroxene (0–60), plagioclase (35–75), hornblende (0–55) and biotite (0–30) with accessory apatite, zircon, sphene and opaque oxide.

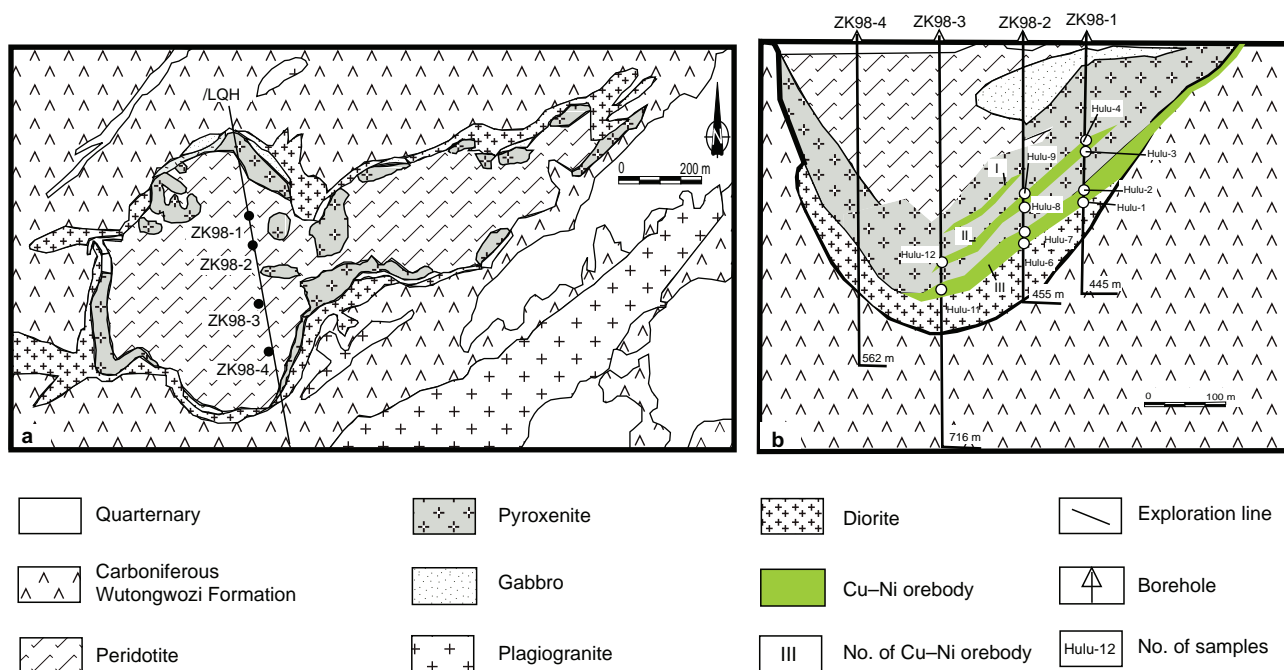


Fig. 3 Plan view (a) and cross-section of exploration line 98 from the Hulu Cu–Ni deposit (b) (modified from Chen et al. 2005).

Alteration minerals include saussurite, carbonate, sericite and biotite.

In addition, a plagiogranite, located in the eastern part of the area, has a porphyritic texture and a massive structure. Phenocrysts are quartz, plagioclase and biotite in a matrix with a subhedral texture. Wall-rock alteration is marked by silicification, sericitization and carbonatization.

#### 4. Geology of the ore deposit

The mine of the Hulu deposit includes six ore bodies of which the No. III and No. IV ore are the largest.

The No. III ore body is oxidized from the surface to depths of more than 30 m. Its orientation is similar to that of the intrusion, which dips to the 30–41° to the SE (Fig. 3). The Cu–Ni sulfide ores are hosted by the pyroxenite unit at depths ranging from 410 to 640 m below the surface (Fig. 3). The ore contains 1835 t Cu, 35666 t Ni, and 1848 t Co based upon average grades of 0.28 % Cu, 0.54 % Ni, and 0.028 % Co.

The No. IV ore body has a strike length of 290 m, a width of between 90 and 280 m, and a depth of 290 m. The Cu–Ni sulfide ores are hosted in the peridotite unit at depths ranging from 330 to 530 m below the surface (Fig. 3). The orientation of the orebody is almost parallel to that of the intrusion, which dips 28° N, and it has an average thickness of 15.44 m (Fig. 3). The ore contains 2785 t Cu, 6321 t Ni, and 309 t Co based upon average

grades of 0.311 % Cu, 0.813 % Ni, and 0.036 % Co (Chen et al. 2005).

Mineralogically, the ore minerals of the Hulu Cu–Ni deposit are predominantly magnetite, pyrrhotite, pentlandite, chalcopyrite with minor gregoryite, chalcocite, hessite and melonite. The gangue minerals are olivine, pyroxene, plagioclase, hornblende, biotite, chlorite and serpentine. The textures of the ore minerals are variably euhedral, subhedral, anhedral, subhedral–anhedral, gabbroic, poikilitic, interstitial and corrosional with reaction rims, and the ore structures are mainly massive, disseminated, sparsely disseminated, spotted and banded.

Based on crosscutting relationships among minerals and mineral assemblages, the mineralization in the Hulu orebody can be divided into four genetic growth stages. Stage 1 is characterized by olivine and spinel and some metal sulfides; magnetite + ilmenite is a representative ore mineral assemblage. Stage 2 included chloritization, serpentinization, epidotization, which gave rise to the characteristic chalcopyrite + pentlandite + pyrrhotite + pyrite assemblage. Stage 3 formed under hydrothermal conditions that led to the diagnostic chlorite + epidote + pyrite + chalcopyrite assemblage. Stage 4 is marked by supergene oxidation, which resulted in the formation of secondary minerals such as malachite, pastreite, ferrosulfate and covellite.

Wall-rock alteration related to mineralization in the Hulu Cu–Ni ore deposit includes chloritization, epidotization, serpentinization, sericitization, tremolitization, biotitization, phlogopitization and amphibolitization (Hu et

al. 2008). Characteristic minerals in the alteration zones are talc, chlorite, serpentine, epidote, actinolite, zoisite, sericite and carbonate.

## 5. Analytical methods

### 5.1. Major- and trace-element analyses

After petrographic examination, fresh rock samples were crushed and powdered in agate mill. Analyses were conducted at the Institute of Geology and Geophysics (IGG), Chinese Academy of Science in Beijing. Major-element analyses were carried out by X-ray Fluorescence (XRF) using a Shimadzu XRF1500 sequential spectrometer at IGG. The precision of the XRF analyses is estimated to be better than 1% for elements present in amounts greater than 200 ppm and 1 to 3% for those less abundant. The trace-element (including REE) concentrations were measured with an Agilent 7500a Inductively Coupled Plasma Mass Spectrometer (ICP-MS). About 50 mg of crushed whole-rock powder were dissolved using HF/HNO<sub>3</sub> (10:1) mixtures in screw-top Teflon beakers for 7 days at ~100 °C, followed by evaporation to dryness, refluxing in 7N HNO<sub>3</sub> to incipient dryness again, and the sample cake was then re-dissolved in 2% HNO<sub>3</sub> to a sample/solution weight ratio of 1:1000. International geochemical standards, GSR-1 (granite), GSR-3 (basalt) and Geo-PT-12 (ultramafic rock), were used for calibration. The accuracies of the ICP-MS analyses are estimated to be better than ± 10 % and precision is normally better than 3 %; further details can be found in Gao et al. (2002).

### 5.2. Zircon separation and CL imaging

After sample crushing, zircons were separated by standard heavy liquid and magnetic techniques. Zircon grains from the >25 μm non-magnetic fractions were hand-picked and mounted on adhesive tape, then enclosed in epoxy resin and polished to about half their thickness. After being photographed under reflected and transmitted light, the samples were prepared for cathodoluminescence (CL) imaging and U–Pb dating.

All zircons were documented with transmitted and reflected light micrographs as well as with CL images to reveal their internal structures using a CAMECA SX-50 electron microprobe at the IGG.

### 5.3. Re–Os isotopes

For Re–Os dating, we collected ten samples from three representative boreholes (Zk98–1, ZK98–2 and ZK98–3) in the Hulu orebody (Fig. 3). They were crushed, split

and ground to < 100 mesh. Sample preparation and mineral separation were done using techniques outlined in Mao et al. (2002).

The Re–Os isotopic analyses were performed at the National Research Center of Geoanalysis. The details of the chemical procedure have been described by Shirey and Walker (1995), Stein et al. (1998) and Markey et al. (1998), and are briefly summarized below.

Enriched <sup>190</sup>Os and enriched <sup>185</sup>Re were obtained from the Oak Ridge National Laboratory, USA. Using a Carius tube (a thick-walled borosilicate glass ampoule) digestion the weighed samples were loaded in the Carius tube through a thin-necked long funnel. The mixed <sup>190</sup>Os and <sup>185</sup>Re spike solutions and 2 ml of 12M HCl and 6 ml of 15M HNO<sub>3</sub> were loaded while the bottom part of the tube was frozen at –80 °C to –50 °C in an ethanol–liquid nitrogen slush. The top was sealed using an oxygen–propane torch. The tube was then placed in a stainless-steel jacket and heated for 24 hours at 230 °C. Upon cooling, the bottom part of the tube was refrozen, the neck of the tube was broken, and its contents were poured into a distillation flask and the residue was washed out with 40 ml of water.

Osmium was distilled at 105–110 °C for 50 minutes and trapped in 10 ml of water. The residual Re-bearing solution was saved in a 150 ml Teflon beaker for late Re separation. The water trap solution was used for ICP-MS (TJA X-series) determination of the Os isotope ratio.

The Re-bearing solution was evaporated to dryness, and 1 ml of water was added twice. Following heating to near-dryness, 10 ml of 20% NaOH were added to the residue, prior to Re extraction with 10 ml of acetone in a 120 ml Teflon separation funnel. The water phase was then discarded and the acetone phase washed with 2 ml of 20% NaOH. The acetone phase was transferred to a 120 ml Teflon beaker that contained 2 ml of water. After evaporation to dryness, the Re was picked up in 1 ml of water that was used for the ICP-MS determination of the Re isotope ratio. Cation-exchange resin was used to remove Na when the salinity of the Re-bearing solution was more than 1 mg/ml (Du et al. 2004).

The ICP-MS analysis was conducted on a TJA PQ ExCELLICP mass spectrometer. The instrument was optimized to more than 5×10<sup>4</sup> cps for 1 ng ml<sup>-1</sup> <sup>115</sup>In and more than 5×10<sup>4</sup> cps for 1 ng ml<sup>-1</sup> <sup>238</sup>U. Data acquisition was performed in peak-jumping mode, 3 points/u; dwell time was 15 ms/point and number of scans 200 for 5 ppb of Re in solution. The reproducibility by ICP-MS is 0.3% (RSD, 2S, n = 5); by using water as an absorbent for OsO<sub>4</sub>, the sensitivity of Os by ICP-MS increased significantly. For 0.2 ppb of Os solution, the reproducibility is 0.3% (RSD, 2S, n = 5).

If a minor <sup>190</sup>Os signal was observed when measuring Re, the <sup>187</sup>Re signal was appropriately corrected for

$^{187}\text{Os}$  using the  $^{187}\text{Os}/^{190}\text{Os}$  ratio of the spiked Os solution. Conversely, if a minor  $^{185}\text{Re}$  signal was observed while analyzing the Os-bearing solution,  $^{187}\text{Os}$  was appropriately corrected for  $^{187}\text{Re}$  using the measured  $^{185}\text{Re}/^{187}\text{Re}$  of the spiked sample. The corrections were generally minor and constituted no more than 0.1 % of the isotope signal. The maximum correction percentage that we used was always less than 1 %.

The mass fractionation can be corrected by an inter laboratory isotope reference standard. Using the  $\lambda^{238}\text{U}$  value of Jaffey et al. (1971) and  $\lambda^{235}$  value of Schoene et al. (2006), a value for  $\lambda^{187}\text{Re}$  of  $1.6689 \pm 0.0031 \times 10^{-11} \text{a}^{-1}$  was determined. This is nominally higher (c. 0.1 % and c. 0.2 %) than that presented by Smoliar et al. (1996), but within the calculated uncertainty. So, we used the  $\lambda^{187}\text{Re}$   $1.666 \pm 0.005 \times 10^{-11} \text{a}^{-1} \pm 0.017$  (1.0 %) of Smoliar et al. (1996).

The uncertainty in each individual age determination was c. 1.02 % including the uncertainty of the decay constant of  $^{187}\text{Re}$ , uncertainty in isotope ratio measurement, and spike calibrations.

Average blanks for the total Carius tube procedure as described above were c. 10 pg Re, and c. 0.1 pg Os;  $^{187}\text{Os}$  was not detected. Three reference materials were used to check the analytical results. The blanks for the total Carius tube procedure are listed in Tab. 2 and the results are in Tab. 3.

#### 5.4. U–Pb zircon geochronology

The zircon mount was vacuum-coated with high-purity gold prior to secondary ion mass spectrometry (SIMS) analysis. Measurements of U, Th and Pb were made with a Cameca IMS-1280 SIMS at the IGG. The U–Th–Pb ratios and absolute abundances were determined relative to the standard zircon 91500 (Wiedenbeck et al. 1995), analyses of which were interspersed with those of unknown grains, using operating and data processing procedures similar to those described by Li et al. (2009). The mass resolution used to measure Pb/Pb and Pb/U isotopic ratios was 5400 during the analyses. A long-term uncertainty of 1.5% (1 RSD) for  $^{206}\text{Pb}/^{238}\text{U}$  measurements of the standard zircons was propagated to the unknowns (Li et al. 2010), despite the fact that the measured  $^{206}\text{Pb}/^{238}\text{U}$  error in a specific session was generally around 1% or less. Measured compositions were corrected for common Pb using non-radiogenic  $^{204}\text{Pb}$ . Corrections were sufficiently small to be insensitive to the choice of common Pb composition, and an average of present-day crustal composition (Stacey and Kramers 1975) was used for the common Pb assuming that the common Pb is largely surface contamination introduced during sample preparation. Uncertainties on individual analyses in data tables are reported at a 1 RSD level;

mean ages for pooled U/Pb (and Pb/Pb) analyses are quoted with 95% confidence interval. Data reduction was carried out using the Isoplot/Ex v. 2.49 program (Ludwig 2001).

## 6. Results

### 6.1. Major- and trace-element geochemistry

The mafic and ultramafic rocks hosting the Hulu Cu–Ni ore bodies show a wide variation in their major oxide concentrations (Tab. 2). The representative samples have a wide range of  $\text{SiO}_2$  (29.67–56.14 wt. %),  $\text{MgO}$  (2.70–35.03 %) and  $\text{Al}_2\text{O}_3$  (3.36–17.97 %) contents, and have relatively low  $\text{TiO}_2$  (0.12–1.80 %) and  $\text{K}_2\text{O} + \text{Na}_2\text{O}$  (0.06–5.41 %) contents (Tab. 2).

The Hulu intrusion underwent regional low amphibolite-facies metamorphism and intrusion-related alteration, which limit the use of fluid-soluble elements for petrogenetic study, but high field strength elements (HFSE; REE, Y, Ti, Zr, Hf, Nb, Ta, Th, and P) and some transition metals (Co, Ni, V, Sc, and Cr) are generally considered immobile during such processes (Pearce 1996). Our conclusions focus on the relatively immobile elements and are not based on the altered samples. This is supported by tight clusters of HFSE in normalized trace-element plots (Fig. 4). The REE patterns are also mutually comparable except for minor scatter in LREE (Fig. 5), consistent with their relatively high mobility in hydrothermal fluids. Therefore, we assume that with prudence, the samples can provide useful information on the primary geochemistry of the Hulu intrusion.

Almost all the rocks have subparallel chondrite-normalized REE patterns (Fig. 5). The samples have variable REE contents, reflecting different abundances and compositions of intercumulus liquids, but are uniformly enriched in LREE relative to HREE, with  $(\text{La}/\text{Yb})_{\text{N}}$  of 1.05–3.09 and flat HREE chondrite-normalized patterns with  $(\text{Gd}/\text{Yb})_{\text{N}} = 1.11–1.81$  (Fig. 5; Tab. 2). Most rocks have slightly negative Eu anomalies ( $\text{Eu}/\text{Eu}^* = 0.79$  to 1.21), which may be attributed to the fractionation/ac-cumulation of plagioclase.

Primitive mantle-normalized diagrams exhibit variable incompatible elements concentrations, reflecting probably the different abundances and compositions of intercumulus liquids (Fig. 4). The contents of more incompatible large ion lithophile elements (LILE) are greater than those of the HFSE. This is typical of the crust and magmas proposed to possess a strong enriched mantle component. Other notable features include the depletion in Nb and Ta relative to La and U, enrichment of Zr relative to Gd and Eu, and depletion of Eu relative to Rb and U (Fig. 4).

**Tab. 2** Major- and trace-element data of the Hulu Complex

Sample No.	Hulu16	Hulu19	Hulu20	Hulu21	Hulu23	Hulu24	Hulu25	Hulu29	J1-1	J1-2	J6-1	J6-2
Lithology	PE	PE	PE	PE	PE	PY	PY	PY	GD	GD	GD	GD
SiO <sub>2</sub>	29.67	38.25	38.67	38.72	38.48	39.28	39.03	38.29	56.14	55.32	47.29	46.92
TiO <sub>2</sub>	0.20	0.13	0.13	0.13	0.13	0.12	0.12	0.24	1.61	1.80	1.45	1.47
Al <sub>2</sub> O <sub>3</sub>	3.86	5.79	5.15	5.85	5.70	5.34	5.46	4.74	14.45	14.74	17.76	17.68
Fe <sub>2</sub> O <sub>3</sub> *	25.46	11.68	12.27	11.63	11.74	11.83	11.87	12.68	9.60	10.34	11.13	11.36
MnO	0.14	0.14	0.15	0.14	0.14	0.15	0.15	0.17	0.18	0.20	0.19	0.19
MgO	23.07	31.37	31.84	32.19	31.44	31.48	31.76	31.37	2.70	3.62	5.14	5.12
CaO	2.70	2.35	2.57	2.40	2.52	2.56	2.43	3.08	9.44	6.82	9.30	9.32
Na <sub>2</sub> O	0.04	0.12	0.14	0.11	0.15	0.11	0.11	0.13	2.93	3.99	4.35	4.22
K <sub>2</sub> O	0.02	0.02	0.02	0.02	0.02	0.02	0.02	0.03	0.47	0.74	1.06	1.02
P <sub>2</sub> O <sub>5</sub>	0.04	0.03	0.03	0.03	0.03	0.03	0.03	0.09	0.34	0.37	0.31	0.31
LOI	9.13	9.85	8.98	8.52	9.45	8.97	9.04	8.96	2.39	2.97	1.58	2.55
∑	94.32	99.73	99.95	99.73	99.80	99.89	100.01	99.78	99.16	100.00	99.35	99.36
Mg <sup>#</sup>	64	84	84	85	84	84	84	83	36	41	48	47
La	2.28	1.58	1.84	1.79	1.63	1.58	1.61	3.04	12.64	13.69	10.19	10.7
Ce	4.57	2.98	3.45	3.55	3.08	3.02	3.05	6.93	29.48	32.95	24.94	26.06
Pr	0.75	0.48	0.54	0.55	0.50	0.49	0.50	1.01	3.86	4.33	3.56	3.68
Nd	3.20	2.04	2.34	2.32	2.18	2.09	2.17	4.55	20.42	23.26	19.92	20.58
Sm	0.83	0.58	0.65	0.66	0.58	0.61	0.62	1.22	5.03	5.95	4.93	5.11
Eu	0.27	0.20	0.23	0.22	0.22	0.21	0.21	0.34	1.86	2.17	1.71	1.82
Gd	0.90	0.59	0.68	0.70	0.62	0.66	0.67	1.29	5.94	6.77	5.28	5.65
Tb	0.15	0.10	0.11	0.11	0.10	0.11	0.11	0.21	0.89	1.08	0.77	0.81
Dy	0.93	0.63	0.74	0.74	0.63	0.69	0.74	1.27	5.50	6.65	4.65	4.83
Ho	0.19	0.13	0.16	0.16	0.13	0.14	0.16	0.26	1.03	1.25	0.84	0.90
Er	0.57	0.38	0.45	0.45	0.39	0.40	0.44	0.72	3.36	4.07	2.75	2.86
Tm	0.09	0.06	0.07	0.07	0.06	0.06	0.07	0.10	0.41	0.52	0.33	0.36
Yb	0.57	0.39	0.43	0.44	0.39	0.41	0.43	0.67	3.02	3.82	2.36	2.53
Lu	0.09	0.06	0.06	0.07	0.06	0.07	0.07	0.10	0.40	0.54	0.32	0.36
∑REE	15.38	10.22	11.75	11.82	10.57	10.53	10.84	21.72	93.84	107.10	82.55	86.25
Sc	9	10	13	9	10	11	13	13	7	34	29	36
Cr	1430	1716	1844	1976	1895	1823	2567	2382	14	12	2	2
Co	481	124	107	103	109	103	111	118	72	54	47	46
Ni	11841	786	654	587	653	593	627	669	0.5	0.3	2	2
Cu	6639	315	169	149	251	123	138	172	44	46	118	135
Ga	4	5	4	5	5	5	5	4	30	36	34	34
Rb	0.5	0.5	0.6	0.6	0.5	0.6	0.7	1.3	8.6	12.6	13.8	19.5
Sr	112	70	69	64	79	67	61	115	531	388	849	839
Y	5	4	5	5	4	5	5	7	22	31	22	22
Zr	27	16	15	16	19	14	13	31	36	133	15	62
Nb	1.5	1.3	1.3	1.3	1.2	1.3	1.2	1.6	4.4	4.2	2.7	2.7
Cs	1.5	0.6	0.4	0.2	0.5	0.7	0.7	0.4	0.6	0.3	0.6	0.63
Ba	28	32	51	35	36	31	30	47	161	273	227	231
Hf	0.8	0.5	0.5	0.6	0.6	0.5	0.5	0.9	1.2	3.8	0.9	2.0
Ta	0.08	0.07	0.07	0.07	0.07	0.07	0.07	0.11	0.06	0.07	0.11	0.10
Tl	0.10	0.06	0.04	0.04	0.05	0.04	0.04	0.05				
Pb	33.6	2.2	2.8	2.0	2.7	2.1	2.4	2.8	6.0	4.5	4.1	4.3
Bi	9.1	0.2	0.2	0.1	0.1	0.1	0.2	0.2				
Th	0.6	0.5	0.4	0.4	0.4	0.4	0.5	0.8	2.0	2.7	1.3	1.5
U	0.2	0.2	0.2	0.1	0.2	0.2	0.2	0.4	0.8	0.9	0.2	0.3
Nb/La	0.7	0.8	0.7	0.7	0.8	0.8	0.8	0.5	0.3	0.3	0.3	0.3
Nb/Ta	19.3	18.0	18.0	18.4	17.6	17.9	17.4	14.9	72.5	59.4	24.3	27.2
Zr/Hf	35.1	30.8	29.4	29.1	33.3	28.0	27.7	32.9	30.4	35.3	17.5	30.7
Ce/Pb	0.1	1.4	1.2	1.8	1.1	1.4	1.3	2.5	4.9	7.3	6.1	6.1
(La/Yb) <sub>N</sub>	2.70	2.73	2.88	2.74	2.82	2.60	2.52	3.06	2.82	2.42	2.91	2.85
(Gd/Yb) <sub>N</sub>	1.27	1.22	1.28	1.28	1.28	1.30	1.26	1.55	1.59	1.43	1.81	1.80
Eu/Eu*	1.05	0.97	0.95	1.02	0.90	0.99	1.01	1.21	0.96	0.96	0.98	0.97

PE = peridotite; PY = pyroxenolite; GD = gabbro-diorite

Tab. 2 continued

Sample No.	J6-3	J3-1	J3-2	J5-1	J5-3	J5-4	J4-1	J4-2	J4-3	J2-1	J2-3	J2-4
Lithology	GD	GA	GA	PY	PY	PY	AP	AP	AP	PE	PE	PE
SiO <sub>2</sub>	47.39	48.77	48.59	38.70	37.74	40.19	40.90	41.08	42.56	40.13	39.68	37.75
TiO <sub>2</sub>	1.41	0.85	0.87	0.13	0.27	0.34	0.16	0.21	0.40	0.27	0.58	0.14
Al <sub>2</sub> O <sub>3</sub>	17.97	17.36	16.98	4.78	4.10	3.81	6.09	5.92	7.90	3.36	3.89	3.39
Fe <sub>2</sub> O <sub>3</sub> *	11.10	10.28	10.43	10.59	13.61	11.77	10.47	11.47	10.19	11.51	12.11	12.27
MnO	0.18	0.17	0.17	0.13	0.15	0.13	0.15	0.15	0.16	0.17	0.18	0.15
MgO	5.08	6.83	6.96	32.71	30.62	31.82	29.19	28.44	25.49	33.42	33.80	35.03
CaO	9.27	9.97	10.08	1.92	2.02	1.96	3.67	4.19	5.08	3.10	2.38	1.43
Na <sub>2</sub> O	4.34	3.70	3.65	0.19	0.10	0.11	0.16	0.19	0.24	0.41	0.36	0.06
K <sub>2</sub> O	1.07	0.68	0.76	0.06	0.04	0.04	0.02	0.02	0.05	0.05	0.06	0.02
P <sub>2</sub> O <sub>5</sub>	0.31	0.06	0.06	0.02	0.05	0.06	0.03	0.01	0.07	0.04	0.06	0.03
LOI	1.88	2.62	2.54	19.90	19.71	18.56	17.61	16.24	13.66	13.67	12.52	19.51
Σ	99.52	100.4	100.1	99.95	99.53	100.10	100.6	100.4	99.64	100.1	100.17	99.81
Mg#	48	57	57	86	82	84	85	83	83	85	85	85
La	9.81	3.60	3.86	1.01	2.43	2.64	1.74	0.70	2.97	2.34	3.26	1.44
Ce	24.15	8.23	10.21	2.31	5.57	6.26	3.58	1.79	7.46	5.41	7.35	2.97
Pr	3.44	1.14	1.21	0.30	0.70	0.79	0.43	0.28	1.02	0.68	0.92	0.38
Nd	19.42	6.22	6.75	1.53	3.47	3.97	2.11	1.72	5.54	3.58	4.61	1.87
Sm	4.91	1.66	1.86	0.43	0.84	0.95	0.53	0.54	1.47	0.90	1.23	0.45
Eu	1.71	0.78	0.78	0.18	0.25	0.29	0.16	0.24	0.55	0.29	0.37	0.15
Gd	5.18	2.14	2.20	0.51	1.02	1.18	0.65	0.62	1.67	1.10	1.48	0.55
Tb	0.75	0.32	0.34	0.08	0.15	0.17	0.10	0.11	0.26	0.17	0.23	0.09
Dy	4.62	2.13	2.18	0.55	0.97	1.15	0.65	0.74	1.70	1.08	1.50	0.58
Ho	0.82	0.40	0.41	0.10	0.18	0.22	0.13	0.14	0.32	0.21	0.28	0.11
Er	2.65	1.32	1.33	0.32	0.59	0.72	0.39	0.44	1.02	0.69	0.91	0.35
Tm	0.34	0.16	0.17	0.05	0.08	0.09	0.05	0.06	0.14	0.09	0.11	0.05
Yb	2.36	1.16	1.20	0.32	0.53	0.74	0.38	0.45	0.99	0.65	0.85	0.37
Lu	0.35	0.17	0.17	0.05	0.08	0.10	0.05	0.06	0.14	0.09	0.12	0.06
ΣREE	80.51	29.44	32.67	7.74	16.86	19.27	10.95	7.87	25.25	17.28	23.22	9.42
Sc	19	41	42	21	20	19	15	24	26	25	21	12
Cr	2	116	129	2599	2635	2519	2191	2393	2024	2562	2684	2727
Co	39	51	48	101	177	106	84	97	91	112	117	112
Ni	1	42	43	492	2967	599	437	410	483	545	587	617
Cu	103	51	37	129	1521	140	65	85	24	48	84	22
Ga	34	27	25	6	6	5	6	10	9	5	5	58
Rb	20.9	9.6	9.9	2.9	1.0	1.2	0.4	0.5	1.3	0.8	1.1	0.4
Sr	880	714	623	66	47	30	45	52	89	83	72	38
Y	20	10	11	3	5	6	3	15	8	6	8	3
Zr	52	33	36	10	26	36	14	13	56	26	38	15
Nb	2.5	0.8	0.9	0.3	0.8	1.3	0.3	0.4	1.1	0.7	1.5	0.4
Cs	0.62	0.76	1.63	2.24	1.65	1.11	0.04	0.04	1.53	0.07	0.26	0.55
Ba	230	158	137	9	7	8	5	70	10	9	12	8
Hf	1.8	1.0	1.1	0.3	0.7	1.0	0.4	0.4	1.3	0.7	1.1	0.4
Ta	0.11	0.20	0.19	0.02	0.02	0.02	0.04	0.04	0.02	0.01	0.04	0.04
Tl												
Pb	4.1	2.4	2.1	1.3	6.7	1.3	0.6	0.6	1.8	1.7	1.8	2.3
Bi												
Th	1.3	1.1	1.4	0.6	1.0	1.3	0.6	0.7	1.3	0.9	1.2	0.7
U	0.2	0.3	0.3	0.1	0.2	0.2	1.8	1.1	0.4	0.2	0.4	0.1
Nb/La	0.3	0.2	0.2	0.3	0.3	0.5	0.2	0.6	0.4	0.3	0.4	0.3
Nb/Ta	23.1	4.0	4.6	13.0	39.5	63.5	6.8	9.8	56.5	73.0	36.3	9.5
Zr/Hf	29.6	33.1	33.3	35.3	36.1	36.1	34.1	31.9	42.9	35.8	36.2	35.5
Ce/Pb	5.9	3.5	4.8	1.8	0.8	4.7	6.2	2.8	4.2	3.2	4.1	1.3
(La/Yb) <sub>N</sub>	2.80	2.09	2.17	2.13	3.09	2.41	3.09	1.05	2.02	2.43	2.59	2.62
(Gd/Yb) <sub>N</sub>	1.77	1.49	1.48	1.29	1.55	1.29	1.38	1.11	1.36	1.37	1.41	1.20
Eu/Eu*	0.97	0.79	0.85	0.85	1.21	1.19	1.20	0.79	0.93	1.12	1.19	1.09

GD = gabbro–diorite; GA = gabbro; AP = augite peridotite; PE = peridotite

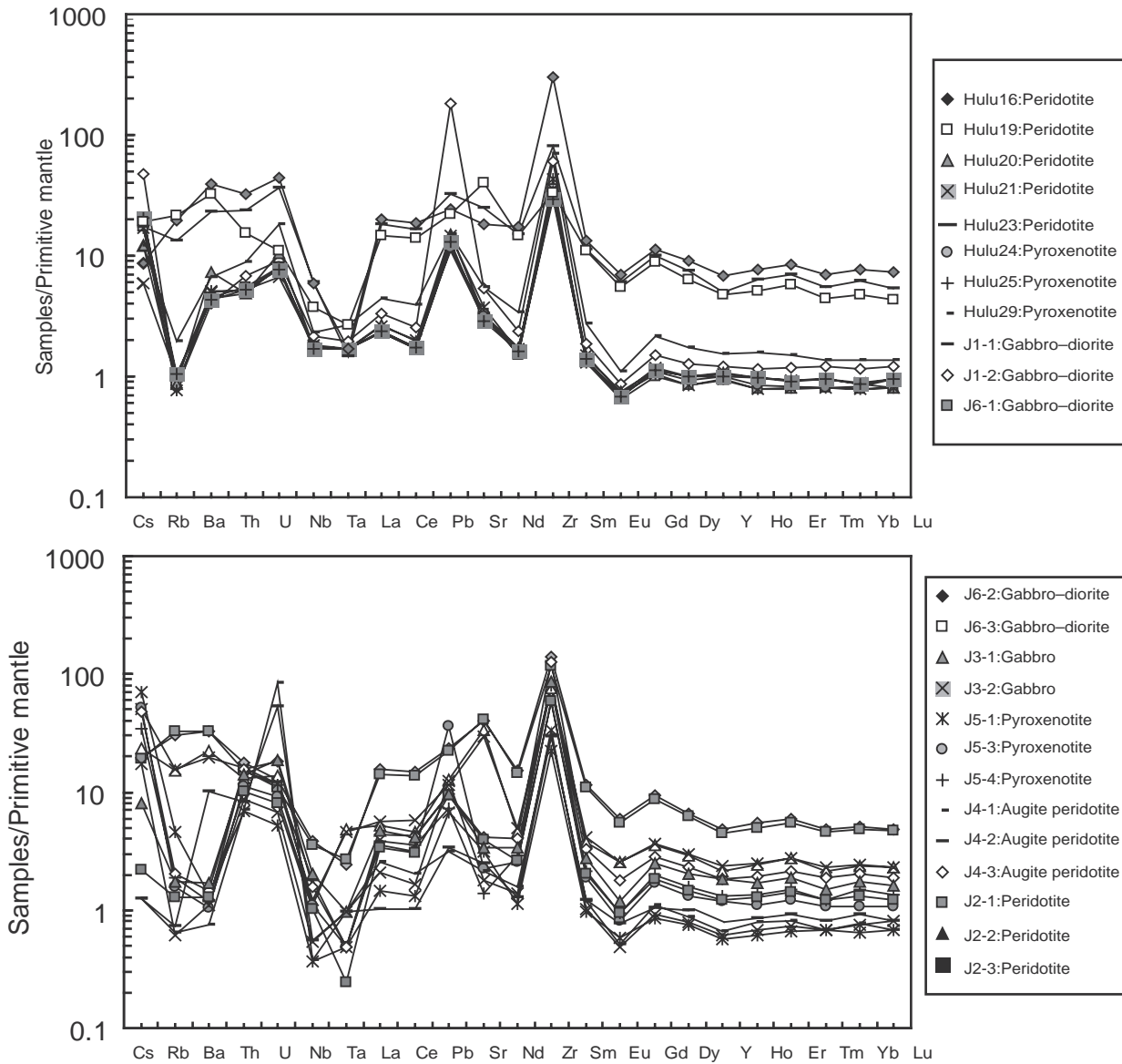


Fig. 4 Primitive mantle-normalized trace element spidergrams for the Hulu Complex (normalization values are from Sun and McDonough 1989).

### 6.2. Zircon U–Pb ages

Samples in this study were all collected from the representative borehole (Zk 98-2) from the Hulu intrusion. Zircons from the dated gabbro sample (GA) are mostly small, euhedral and colorless. This sample consists of 30 % pyroxene, 40–50 % plagioclase, green hornblende, brown biotite and apatite, spinel, chromite as well. Poikilitic textures can be observed whereby large hornblende crystals include numerous inclusions of pyroxene, plagioclase, apatite and opaque oxide. Plagioclase crystals are often replaced by granular saussurite and fine-grained clay minerals.

In CL images (Fig. 6), no inherited cores were observed. The zircons have high U (529–6117 ppm) and

Th (32–18 382 ppm) contents, and high Th/U ratios (0.08–3.34) (Tab. 3). Such features indicate that they crystallized from magmas (Wu and Zheng 2004). Fifteen analyses of 13 zircon grains (Tab. 3) form a tight cluster on Concordia, yielding a weighted mean  $^{206}\text{Pb}/^{238}\text{U}$  age of  $282.3 \pm 1.2$  Ma (95% confidence level, MSWD = 3.30, Fig. 7), which we interpret to be the best estimate of the crystallization age of the gabbros (Early Permian).

### 6.3. Re–Os isotopes

The Re and Os concentrations with  $^{187}\text{Re}/^{188}\text{Os}$  and  $^{187}\text{Os}/^{188}\text{Os}$  ratios of the Hulu sulfide ores, corrected for blanks, are listed in Tab. 4. The sulfide samples show Re and  $^{187}\text{Os}$  concentrations of 36–91 ppb and 0.5–1.1 ppb,

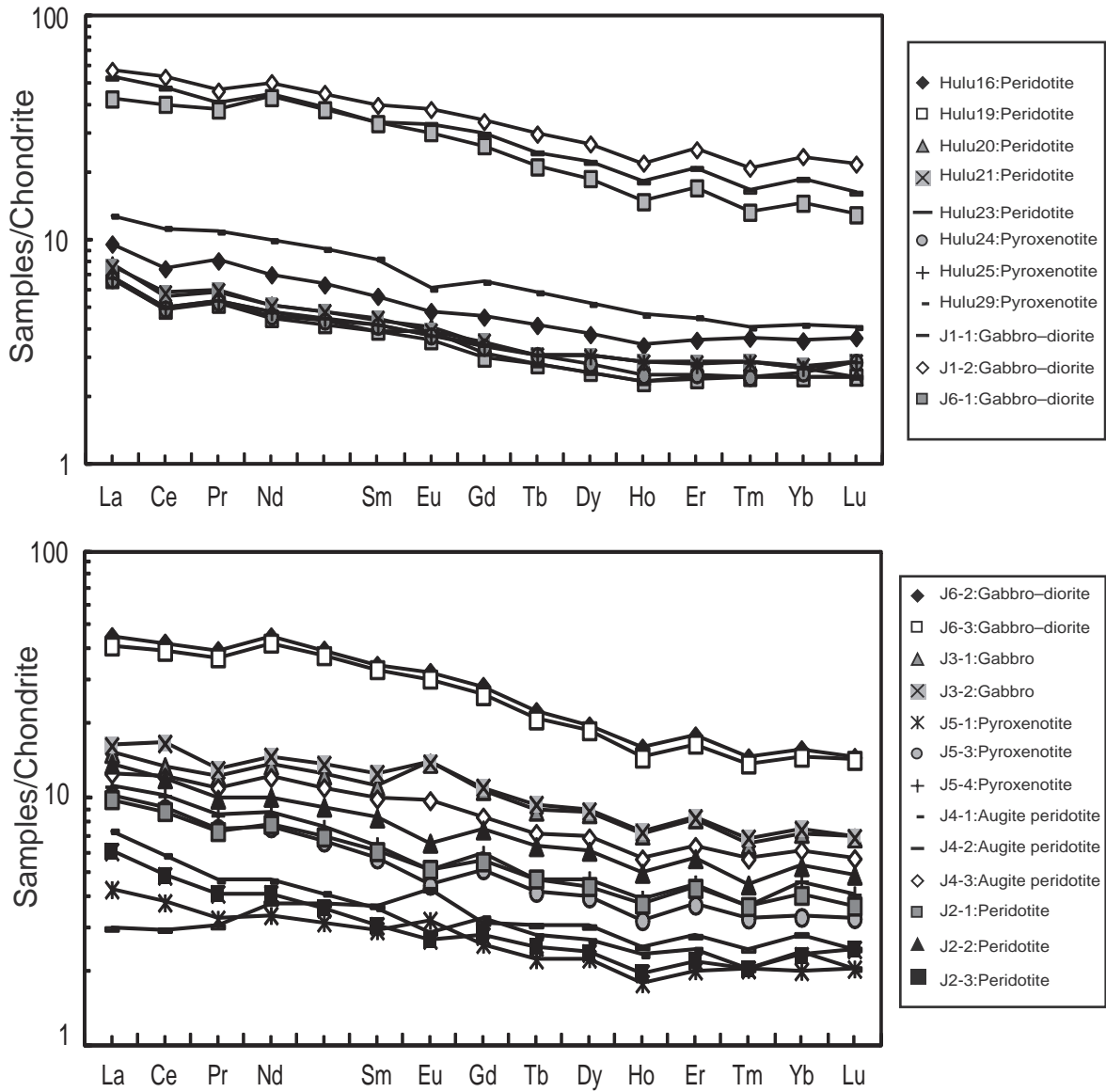


Fig. 5 Chondrite-normalized REE patterns from a suite of rocks of the Hulu Complex (chondrite-normalization values are from Sun and McDonough 1989).

respectively. The initial  $^{187}\text{Os}/^{188}\text{Os}$  ratios range from 1.41 to 1.97 and the calculated  $\gamma\text{Os}$  values from 1023 to 1473.

## 7. Discussion

### 7.1. Timing of Cu–Ni mineralization in Northern Xinjiang

The western part of the southern CAOB includes a large number of ore deposits, of which the most prominent are the Jingbulake deposits in western Tianshan, the Kalatongke deposits in eastern Junggar, the Huangshan, Huangshandong, Xiangshan, Hulu and Tulaergen deposits along the Kanggurtag suture in the Chinese eastern

Tianshan, the Baishiquan, Tianyu and Tianxiang deposits along the southern segment of the Aqikkuduk Fault in the Central Tianshan, and the Poyi, Poshi, Luodong and Hongshishan deposits in the southern sector of the Baidiwa Fault in the Beishan orogenic belt (Fig. 1). The time of formation of many of these ore deposits and associated intrusions is well constrained. Most geochronological data for the Cu–(Ni) deposits in northern Xinjiang are whole-rock K–Ar and Sm–Nd ages, and only a few Re–Os and U–Pb ages.

A pyroxene diorite from the Jingbulake intrusion has a SHRIMP zircon U–Pb age of  $434 \pm 6$  Ma (Zhang et al. 2007). The Kalatongke Cu–Ni sulphide ores yielded Re–Os ages of 305–282 Ma (Zhang et al. 2005; Han et al. 2007), and Cu–Ni sulfide ores from the Huangshandong,

**Tab. 3** Zircon U–Pb data determined by monocollector SIMS mode of gabbro from the Hulu magmatic Cu–Ni deposit

Sample spot	U (ppm)	Th (ppm)	Th/U	$f_{206}^{\#}$ (%)	$\frac{^{207}\text{Pb}}{^{206}\text{Pb}}$	$\pm 2\sigma$ (%)	$\frac{^{207}\text{Pb}}{^{235}\text{U}}$	$\pm 2\sigma$ (%)	$\frac{^{206}\text{Pb}}{^{238}\text{U}}$	$\pm 2\sigma$ (%)	$t_{207/235}$ (Ma)	$\pm 2\sigma$	$t_{206/238}$ (Ma)	$\pm 2\sigma$
HL-1	1546	133	0.080	0.03	0.0523	0.67	0.3195	1.68	0.0443	1.54	281.5	4.1	279.4	4.2
HL-3	887	32	0.030	0.04	0.0523	0.91	0.3198	1.87	0.0443	1.63	281.8	4.6	279.7	4.5
HL-4	1397	585	0.480	0.02	0.0512	0.94	0.3151	1.86	0.0447	1.60	278.1	4.5	281.7	4.4
HL-5	819	1855	2.223	0.04	0.0519	0.94	0.3200	2.02	0.0447	1.79	281.9	5.0	281.7	4.9
HL-6	2306	3823	1.756	0.03	0.0517	0.57	0.3315	1.71	0.0465	1.62	290.7	4.3	293.3	4.6
HL-7	6117	5218	0.823	0.02	0.0521	0.35	0.3258	1.76	0.0454	1.73	286.4	4.4	286.0	4.8
HL-8	2392	392	0.135	0.03	0.0526	0.70	0.3127	1.82	0.0431	1.68	276.3	4.4	272.1	4.5
HL-10	1498	397	0.262	0.05	0.0518	0.87	0.3184	1.95	0.0446	1.74	280.7	4.8	281.0	4.8
HL-11	2696	981	0.344	0.01	0.0523	0.53	0.3181	1.65	0.0441	1.56	280.5	4.0	278.2	4.3
HL-12	4692	18382	3.337	0.01	0.0522	0.42	0.3218	1.62	0.0447	1.56	283.3	4.0	282.1	4.3
HL-13	529	296	0.614	0.15	0.0513	1.59	0.3221	2.19	0.0455	1.50	283.5	5.4	287.1	4.2
HL-14	1625	1759	0.977	0.08	0.0525	0.72	0.3208	1.71	0.0443	1.55	282.6	4.2	279.5	4.2
HL-15	1041	889	0.847	0.06	0.0519	1.18	0.3194	2.06	0.0446	1.69	281.4	5.1	281.3	4.7

$f_{206}^{\#}$  is the percentage of common  $^{206}\text{Pb}$  in the total  $^{206}\text{Pb}$

Xiangshan, Hulu and Tulaergen deposits of 298–265 Ma (Mao et al. 2002; Zhang et al. 2005; Li YC et al. 2006). SHRIMP U–Pb ages of the Kalatongke, Huangshandong, Huangshan, Baishiquan, Poshi, and Poyi mineralized

intrusions range between 284 Ma and 276 Ma (Han et al. 2004; Zhou et al. 2004; Wu et al. 2005; Jiang et al. 2006; Li HQ et al. 2006; Han et al. this volume). Except for the Jingbulake deposit, the magmatism and associated

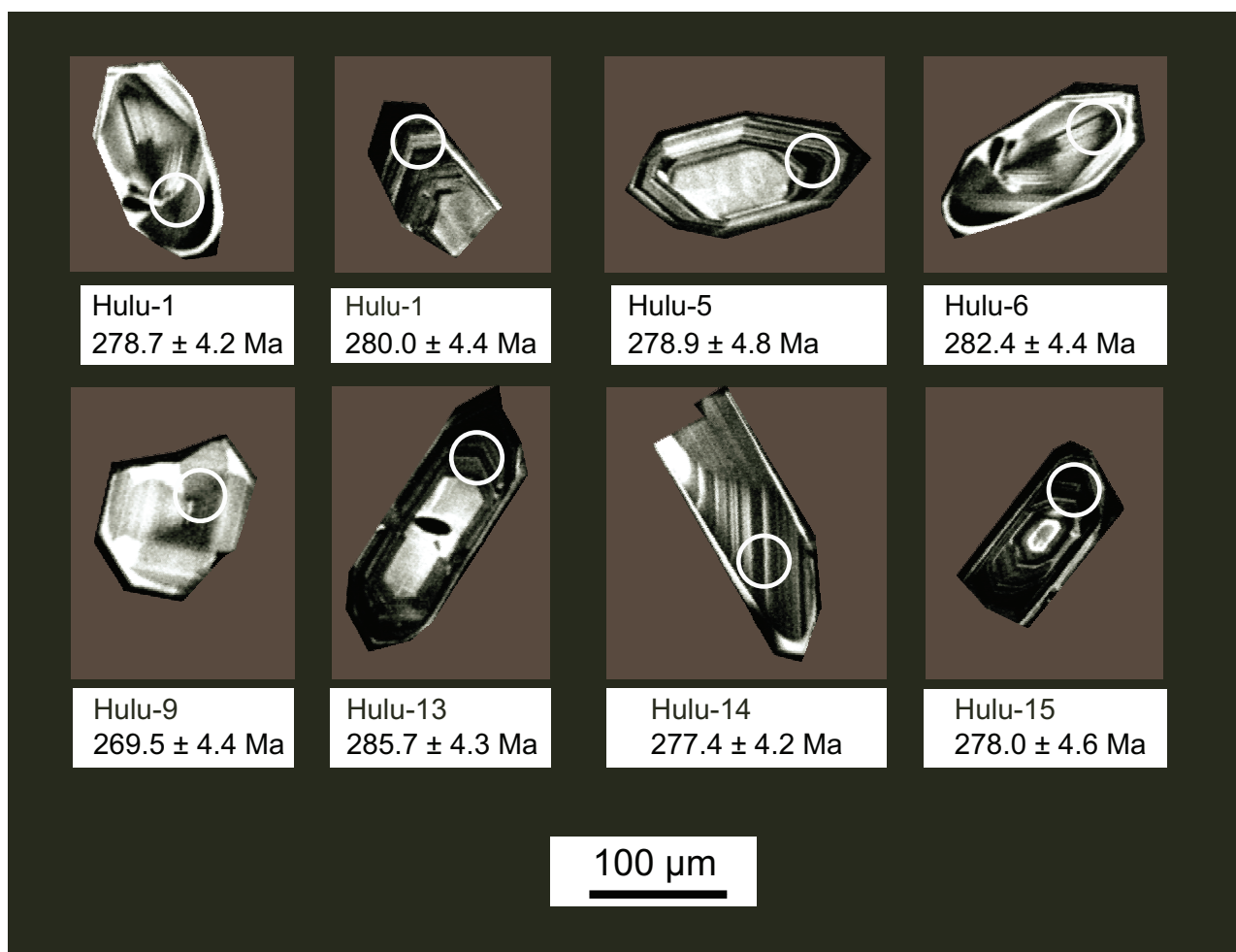


**Fig. 6** Cathodoluminescence images of typical zircon grains from the studied gabbro sample GA from the Hulu Complex.

Tab. 4 Re–Os isotope data for the Cu–Ni sulfide ores from the Hulu deposit

Sample number	Sample weight (g)	Re (ppb) (2σ) <sup>a</sup>	Total Os (ppb) (2σ)	Common Os (ppb) (2σ) <sup>a</sup>	<sup>187</sup> Os (ppb) (2σ)	Re/Os	<sup>187</sup> Re/ <sup>188</sup> Os (2σ)	<sup>187</sup> Os/ <sup>188</sup> Os (2σ) <sup>b</sup>	<sup>187</sup> Os/ <sup>188</sup> Os(t)	γOs	Lithology description	Ore type	Mineral association
Hulu-1	1.201	56.14 (1.33)	1.66 (0.05)	1.21 (0.04)	0.472 (0.01)	46.43	224.2 (8.9)	3.00 (0.12)	1.94	1450	Gabbro	Massive	Pentlandite, chalcopyrite, bornite
Hulu-2	1.201	36.36 (0.43)	1.94 (0.06)	1.51 (0.05)	0.458 (0.01)	24.11	116.5 (3.9)	2.33 (0.09)	1.78	1324	Gabbro	Veinlet	Pentlandite, chalcopyrite, bornite
Hulu-3	0.303	38.15 (0.48)	1.65 (0.02)	1.26 (0.01)	0.416 (0.01)	30.35	146.6 (2.4)	2.54 (0.03)	1.85	1378	Gabbro	Net-textured	Pentlandite, chalcopyrite, pyrite
Hulu-4	1.200	43.47 (0.48)	1.83 (0.03)	1.380 (0.03)	0.481 (0.01)	31.61	152.7 (3.3)	2.69 (0.06)	1.97	1473	Pyroxenite	Net-textured	Pentlandite, chalcopyrite
Hulu-6	1.201	82.51 (1.19)	1.76 (0.05)	1.25 (0.04)	0.557 (0.01)	66.22	319.8 (10.2)	3.32 (0.12)	1.80	1341	Pyroxenite	Disseminated	Pentlandite, chalcopyrite
Hulu-7	1.200	34.41 (0.51)	5.59 (0.24)	4.59 (0.20)	1.088 (0.04)	7.50	36.2 (1.7)	1.82 (0.10)	1.65	1220	Pyroxenite	Massive	Pentlandite
Hulu-8	1.201	81.83 (1.80)	2.90 (0.04)	2.25 (0.03)	0.697 (0.01)	36.37	175.7 (4.4)	2.38 (0.03)	1.55	1138	Peridotite	Disseminated	Pentlandite, chalcopyrite
Hulu-9	0.500	49.97 (0.71)	1.92 (0.02)	1.46 (0.02)	0.4903 (0.01)	34.22	165.3 (3.0)	2.58 (0.03)	1.80	1338	Peridotite	Net-textured	Pentlandite, chalcopyrite
Hulu-11	1.200	60.43 (0.53)	2.14 (0.02)	1.65 (0.02)	0.5201 (0.01)	36.66	177.1 (2.5)	2.43 (0.03)	1.59	1169	Peridotite	Net-textured	Pentlandite
Hulu-12	1.199	90.69 (2.44)	1.95 (0.04)	1.45 (0.03)	0.5336 (0.01)	62.77	303.2 (10.1)	2.84 (0.07)	1.41	1023	Peridotite	Disseminated	Pentlandite, chalcopyrite, bornite

(1)  $Os_{Total} = Os_{Common} + Os_{187}^{187} - Os_{187}^{Common}$ , where  $Os_{187}^{Common} = Os_{Common} \times 0.01926$ ;

(2) Os in Re/Os is common Os. Common Os and common <sup>187</sup>Os are calculated according to the Nier value;

(3) The calculation formula is  $\gamma Os = 100[(^{187}Os/^{188}Os)_{sample} / (^{187}Os/^{188}Os)_{chondrite} - 1]$ ;

where  $(^{187}Os/^{188}Os)_{chondrite} = 0.09531 + 0.40186(e^{2\lambda t} - e^{-\lambda t}) = 0.12512$  at 282.3 Ma, using the <sup>187</sup>Re decay constant of  $\lambda = 1.666 \times 10^{-11} \text{ year}^{-1}$ ;

<sup>a</sup> Re and Os uncertainty < 1 % at 2 standard errors of the mean, including error samples and spike weighting, spike calibration, mass spectrometric analysis, fractionation correction and measured isotope ratios in the samples;

<sup>b</sup> <sup>187</sup>Os/<sup>188</sup>Os uncertainty < 1 % at 2 standard errors of the mean, including error in mass spectrometric analysis, fractionation correction and measured isotope ratios in the samples

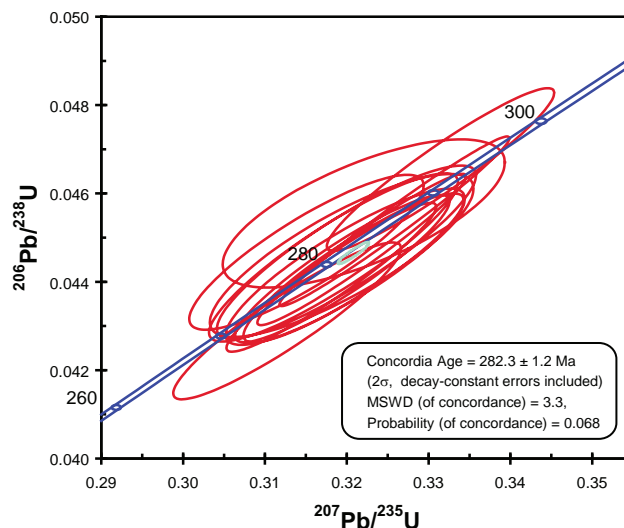


Fig. 7 U–Pb Concordia diagram for zircons from the Hulu gabbro.

magmatic Cu–Ni mineralization seems to have occurred between the Late Carboniferous and Early Permian (Han et al. 2010).

The zircon U–Pb data indicate that the Hulu ultramafic intrusion and associated Cu–Ni sulfide deposit formed at *c.* 282 Ma. The Re–Os ages of the massive ores from Hulu (283 ± 13 Ma, Chen et al. 2005) agree within analytical uncertainties with the zircon U–Pb ages (Tab. 5).

## 7.2. Evidence for crustal contamination

Crustal contamination, which possibly provides both metals and sulfur, is critical for the formation of magmatic sulfide deposits (Naldrett 2004). Wall-rock assimilation by intrusions is very common in the Eastern Tianshan mafic–ultramafic intrusions (Zhou et al. 2004; Chen et al. 2005). Also in Hulu, olivine websterite contains granitic mylonite blocks. In the contact zone of mafic–ultramafic intrusions with metamorphic country rocks, lherzolite and olivine websterite enclose rounded felsic residual xenoliths. The boundaries of xenoliths are often unsharp or even gradual transitions can be observed.

The ratios of trace elements with similar partition coefficients (e.g. Ce/Pb, Th/Yb) are not affected by the degree of fractional crystallization and partial melting. Thus, the correlation and changes between these ratios can accurately verify the role of contamination (Jiang et al. 2006; Sun et al. 2008). The typical mantle Ce/Pb ratio is 25 ± 5, while the crustal one is mostly less than 15 (Hofmann 1997). The Ce/Pb ratios of the Hulu mafic–ultramafic rocks (0.14–7.3; Tab. 2) are lower than those of the mantle, but close to the crustal values. Some of the HFSE, such as Zr, Hf, and Th, tend to concentrate in the lithosphere, particularly in the crust. Primitive mantle-normalized trace-element patterns show relative

**Tab. 5** Geochronological data for the Cu–Ni sulphide deposits and their host rocks in the eastern Tianshan Orogenic Belt

Name of deposit	Dated mineral/rock	Dating method	Age (Ma)	Data source
Huangshandong	Sulfides	Re–Os isochron	282 ± 20	Mao et al. (2002)
	Ultrabasic–basic complex	Sm–Nd isochron	320 ± 38	Li HQ et al. (1998)
	Cu–Ni sulfide ores	Sm–Nd isochron	314 ± 14	Li HQ et al. (1998)
Huangshan	Diorite	SHRIMP zircon U–Pb	269 ± 2	Zhou et al. (2004)
	Olivine norite	SHRIMP zircon U–Pb	274 ± 3	Han et al. (2004)
	Ultrabasic–basic complex	Sm–Nd isochron	308.9 ± 10.7	Li HQ et al. (1998)
	Cu–Ni sulfide ores	Sm–Nd isochron	305.4 ± 2.4	Li HQ et al. (1998)
Xiangshan	Sulphides	Re–Os isochron	298 ± 7.1	Li HQ et al. (2006)
	Gabbro	SHRIMP zircon U–Pb	285 ± 1.2	Qin et al. (2002)
Baishiquan	Quartz diorite	SHRIMP zircon U–Pb	285 ± 10	Wu et al. (2005)
	Gabbro–diorite	SHRIMP zircon U–Pb	284 ± 9	Wu et al. (2005)
	Gabbro	SHRIMP zircon U–Pb	284 ± 8	Wu et al. (2005)
	Gabbro	LA–ICP–MS	281.2 ± 0.9	Mao et al. (2006)
	Sulphides	Re–Os isochron	286 ± 14	Wang H et al. (2007)
Hulu	Sulphides	Re–Os isochron	283 ± 13	Chen et al. (2005)
Tulaergen	Sulphides	Re–Os isochron	265 ± 9.2	Sun et al. (2006)
	Gabbro	SHRIMP zircon U–Pb	300 ± 3	Sun (2009)
Tianyu	Gabbro	LA–ICP–MS	290.2 ± 3.4	Tang et al. (2009)
	Quartz diorite	SHRIMP zircon U–Pb	285 ± 12	Tang et al. (2009)
Poyi	Gabbro	SHRIMP zircon U–Pb	278 ± 2	Li HQ et al. (2006)
Poshi	Gabbro–diorite	SHRIMP zircon U–Pb	274 ± 4	Jiang et al. (2006)

enrichments of LILE, positive anomalies of Zr and Th, as well as negative anomalies of Nb and Ta (Fig. 6). Furthermore, the regional anomalies of higher LILE/HFSE ratios compared with MORB, chondrite-normalized LREE enrichment and flat HREE patterns, may be the result of crustal contamination.

Crustal rocks tend to have distinctively high Re/Os ratios and, with time, develop highly radiogenic  $^{187}\text{Os}/^{188}\text{Os}$  isotopic compositions. The  $\gamma_{\text{Os}}(t)$  value is thus an important parameter because it is capable of indicating the involvement of crustal material in the metallogenic system (Walker et al. 1994). Initial  $^{187}\text{Os}/^{188}\text{Os}$  values at Hulu are much higher than those of mantle sources (0.1243, Shirey and Walker 1998) but far lower than the average continental crustal value (3.63, Shirey and Walker 1998). The  $\gamma_{\text{Os}}(t)$  values for sulfides in different structured ores range from 1023 to 1473 (Tab. 4). Therefore, high initial  $^{187}\text{Os}/^{188}\text{Os}$  ratios and  $\gamma_{\text{Os}}$  values indicate an addition of a large proportion of crustal material in the parental melts.

On a common Os vs. Re/Os diagram (Fig. 8), the Hulu sulfide ores plot in the fields between Duluth sulfides and S-rich sediments, also suggesting that sulfide-bearing sediments might have been added during formation of the sulfide ores. Moreover, preliminary analyses show that the  $\delta^{34}\text{S}$  of the Hulu sulfide ores range from 1.2 to 6.1 ‰ (Sun, 2009), much higher than the mantle values.

The above data suggest that the Hulu intrusion was contaminated with a certain amount of crustal Os during magma emplacement, differentiation and related

mineralization. We infer that crustal contamination was an important factor in the genesis of these magmatic sulfide deposits.

### 7.3. Tectonic setting of the mafic–ultramafic association

Mafic–ultramafic cumulate rocks may form in the lower oceanic crust in seafloor spreading centers, in the roots of oceanic/continental arcs, in crust–mantle transition zones, in continental layered intrusions, and in small magma chambers within the crust or upper mantle (Loucks 1990). Whole-rock geochemistry and isotopic ratios can provide valuable information for interpreting the tectonic setting

and origin of such mafic–ultramafic cumulates (Eyuboglu et al. 2010).

Generally, the incompatible element pairs Nb–Ta and Zr–Hf have similar geochemical properties, and they do not fractionate during partial melting and fractional crystallization. However, the fractionation of Nb from Ta and Zr from Hf occurs in subduction zones (Stolz et al. 1996). The Nb/Ta ratios (4.6–73) and Zr/Hf ratios (18–43) of the Hulu intrusion differ from those of primitive mantle (18 for Nb/Ta, 37 for Zr/Hf, McDonough and Sun 1995) and crust (11 and 33, respectively, Taylor and McLennan 1985), suggesting that the rocks might be derived from subducted material. The presence of hornblende and biotite in almost all studied rocks indicates that the parental magma contained water, suggesting the involvement of a hydrated slab during magma genesis and/or the occurrence of hydrous melt/fluid metasomatism (Peltonen 1995). Marked enrichments in Pb may be ascribed to the presence of hydrous fluid because this element is soluble in aqueous slab-derived fluids (Seghedi et al. 2004). Additionally, experimental data suggest that the Ce/Pb ratios of a slab-derived fluid would be as low as ~0.1 or even lower (Chung et al. 2001), and the Ce/Pb values less than 20 imply the influence of subduction-related fluids within the asthenosphere (Seghedi et al. 2004). The absence of a negative Ce anomaly indicates that these rocks were not affected by low-temperature alteration (Zou et al. 2000). Therefore, the Ce/Pb ratios (0.14–7.3) in most of these rocks, which are lower than in mantle-derived magmas (e.g. Ce/Pb ~ 25 for average

oceanic basalts), may be due to the incorporation of Pb into the mantle via subduction fluids (Chung et al. 2001). The low Pb isotopic ratios exclude the contribution from subducted sediment because the slight addition of sedimentary material would significantly alter Pb isotopic ratios toward more radiogenic values (De Hollanda et al. 2003). Based on the above-described geochemical features, we infer that upper crustal contamination was negligible during the magma evolution. Instead, source contamination by subduction-related components could have been a significant process during the magma genesis, although contamination by lower crust cannot be ruled out.

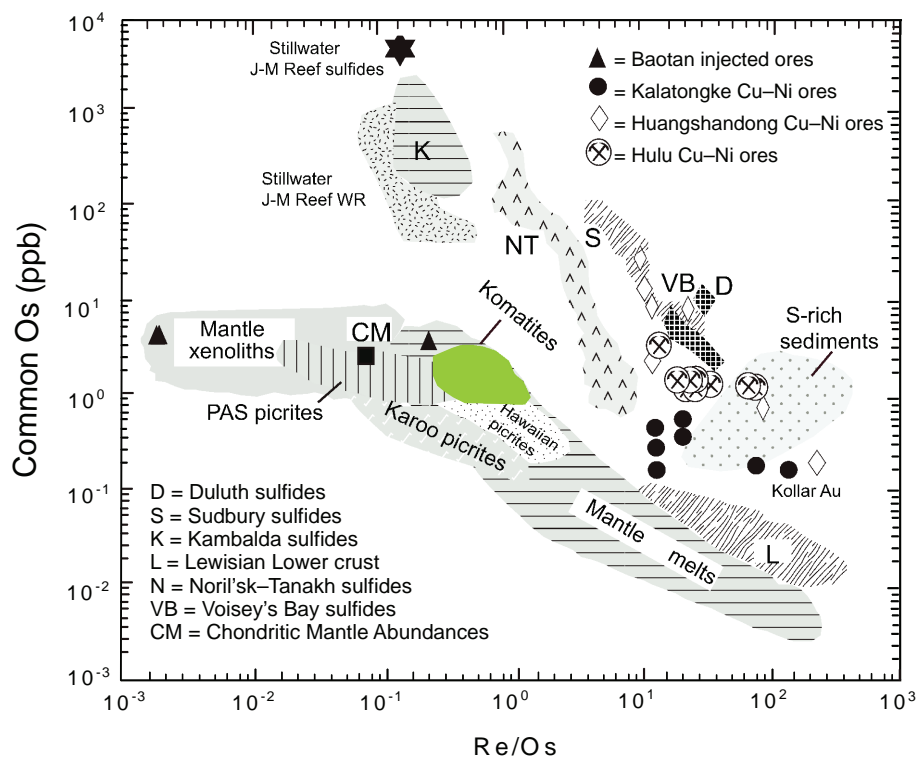
Subduction-related arc magmas are generally characterized by high contents of LILE relative to HFSE and negative Nb, Ta, Hf, Zr, and Ti anomalies (Eyuboglu et al. 2010). The Hulu mafic–ultramafic cumulate rocks are enriched in LILE and LREE, depleted in HFSE and HREE with respect to chondrite and primitive mantle, and show high positive Pb and negative Nb anomalies. These geochemical characteristics indicate that the studied rocks are compositionally similar to subduction-related arc cumulates, particularly in Alaskan-type intrusions (Himmelberg and Loney 1995; Farahat and Helmy 2006).

It is possible that Re and Os may be decoupled from sulfur if they are held within organic matter in C-rich rocks (Ravizza et al. 1991). During devolatilization and conversion of organic C to graphite, both Re and Os can be liberated into a fluid phase. Concentrations in the unmetamorphosed Wutongwozi Fm. hornfels suggest that Re may have been strongly partitioned into the fluid. The effect of incorporation of a Re–Os bearing, but low S fluid

into a source magma would be to elevate  $\gamma_{Os}$  values (Sun 2009), where sulfide saturation is considered to have occurred as a result of subsurface interactions with crustal materials. In fact, the mantle wedge above a subduction zone can be modified by fluids derived from dehydration of altered oceanic crust (Hawkesworth et al. 1993, 1997; Turner et al. 1996) or subducted sediments (Class et al. 2000). The fluids not only modify the mantle composition, but promote melting by decreasing the melting point of the mantle materials (Zhou et al. 2004; Dhuime et al. 2007; Zhao and Zhou 2007). Large spikes in LILE and enrichment of LILE relative to REE and HFSE are common features of aqueous fluid involvement (Plank and Langmuir 1992; Turner et al. 1996; Elliott et al. 1997; Zhao and Zhou 2007).

Our interpretation differs from that of Zhou et al. (2004) and Chai et al. (2008), who proposed that the mafic–ultramafic complexes in the Eastern Tianshan Orogen are part of a Large Igneous Province (LIP) in the Tarim Craton that was the product of a mantle plume within a post-collisional lithospheric delamination and asthenospheric upwelling model, possibly related to slab-break off (Chai et al. 2008). A likely explanation that could reconcile the contrasting models is that the mafic–ultramafic intrusions represent a late-stage evolution of the Dananhu–Tousuquan magmatic arc in the eastern Tianshan Orogen. High-precision ages and isotopic data for the mafic–ultramafic rocks are required to constrain this model, notably in the Eastern Tianshan Orogenic Belt.

**Fig. 8** Re/Os vs. common Os concentration showing data for a PGE-rich sulfide concentrate from the J-M reef, Lower Banded series and basalt associated Cu–Ni sulfide ores from the Basal and Lower Ultramafic series, Stillwater Complex (Lambert et al. 1994), Duluth Complex (Ripley et al. 1999), Sudbury (Walker et al. 1991), Noril'sk–Talnakh (Walker et al. 1994), komatiite-associated Ni sulfide ores from Kambalda (Foster et al. 1996), Archean lithospheric mantle xenoliths from the Kaapvaal and Siberian cratons (Walker et al. 1989); mantle melts, which include komatiites (Walker et al. 1988; Foster et al. 1996) and basalts (Martin 1991; Hauri and Hart 1993; Snow and Reisberg 1995); Lewisian lower crustal gneisses (Frick et al. 1996); metalliferous S-rich sediments (Ravizza and Turekian 1992) and chondritic mantle abundances (Walker and Morgan 1989).



#### 7.4. Implications for exploration in the Eastern Tianshan Orogen

Magmatic sulfide deposits have been broadly classified into sulfur-rich and sulfur-poor (Naldrett 2004). Examples of the former include 1) deposits related to komatiitic magmatism (e.g. Western Australia, Zimbabwe, and the Abitibi Belt of Canada) (Naldrett 2004); 2) deposits in intrusions associated with flood basaltic magmatism (e.g. the Noril'sk region in Siberia and the Emeishan area in SW China; Naldrett 2004); and 3) conduit-related deposits that are broadly assigned to rift zones (e.g. at Voisey's Bay, Canada) (Naldrett 2010). Orogenic convergent plate settings have so far attracted relatively little exploration effort based on theoretical considerations (Maier et al. 2008). However, evidence for an enhanced sulfide potential of magmatic-arc settings has begun to accumulate in the last two decades with the discovery of Cu–Ni ores in the Early Proterozoic Sally Malay intrusion of Australia (Hoatson and Blake 2000), the Early Carboniferous Aguablanca intrusion of Spain (Pina et al. 2006), the Late Carboniferous–Early Permian Kalatongke intrusion of Xinjiang in NW China (Han et al. 2007), the Duke Island Complex in southeastern Alaska (Thakurta et al. 2008), the Tati and Selebi-Phikwe belts of eastern Botswana (Maier et al. 2008) and the Xiangshan intrusion in NW China (Han et al. 2010).

The distribution and geodynamic setting of the Hulu Complex are similar to those of the Alaskan-type intrusions. The Hulu and other eastern Tianshan intrusions form an array along the boundary of the Kangguertag Belt, which is a part of the Kangguertag fore-arc prism (Xiao et al. 2004b).

Alaskan-type complexes are linked to large volumes of subduction zone-related volcanic rocks, and are key components of conduit systems. This dynamic environment would be favorable for the collection of immiscible sulfide liquids that separated from parental magmas. Accreted terrains along tectonic convergence margins provide possible mechanisms of transport of magmas through sulfur-bearing country rocks. Identification of an increasing number of magmatic Cu–Ni sulfide deposits in orogenic settings (including the eastern Tianshan Cu–Ni belts) suggests that the currently-used exploration models for such deposits are incomplete and many orogenic belts in the world should be re-evaluated with regard to their Cu–Ni potential (Maier et al. 2008). This should include convergent margin settings, because these may allow mantle magmas to ascend to upper crustal levels. Subduction-zone environments provide all the necessary conditions suggested by Naldrett (1999) for the generation of world-class Cu–Ni–PGE sulfide deposits. Particularly favorable targets are continental margins where mafic magmas have had the opportunity to interact with sulfide-bearing and graphitic country rocks.

The arc-related geodynamic setting of the eastern Tianshan Cu–Ni deposits is a favorable place for the prospecting of magmatic sulfide deposits. This new type of ore deposit offers an alternative perspective and potential for Cu–Ni exploration. For this reason, it is crucial to better understand the characteristics and origin of the Eastern Tianshan Orogen ore mineralization.

## 8. Conclusions

The Hulu ore body is a magmatic Cu–Ni sulfide deposit in the eastern part of the Central Asian Orogenic Belt. We have obtained a new SIMS U–Pb zircon age of  $282.3 \pm 1.2$  Ma, which gives a minimum age for the emplacement of the main Hulu intrusion.

The initial  $^{187}\text{Os}/^{188}\text{Os}$  ratios (1.41–1.97) and the  $\gamma_{\text{Os}}$  values from the Hulu intrusion (1023 to 1473) suggest that the magma originated from a depleted asthenospheric mantle which underwent some crustal contamination during ascent and subsequent differentiation. Crustal contamination is considered an important mechanism for the concentration of ore-forming elements in mafic–ultramafic systems. The intrusions clearly show island-arc geochemical signatures, such as negative Nb, Ta, Zr and Ti anomalies and enrichment in LILE; these geochemical tracers indicate that the Hulu mafic–ultramafic intrusions, along with the Cu–Ni deposit, formed as a result of subduction of oceanic crust in the Early Permian.

*Acknowledgements.* We are indebted to Xianhua Li, Kezhang Qin, Lianchang Zhang, Tianlin Ma and Jianmin Yang for thoughtful discussions, which improved and initiated many of the ideas in this paper. We are grateful to Brian Windley for his constructive discussions and comments on an early version of the manuscript, which led to substantial improvements. L. Ackerman and an anonymous reviewer are thanked for their constructive comments and proposals. This study was financially supported by funds from the National Natural Science Foundation Projects (41230207, 40725009, 41190072, 41190070, 41272107, 41190071, 41202150, 40421303, and 40572043), the National 305 Projects (2011BAB06B04–1), the One Hundred Talent Program B of the Chinese Academy of Sciences, the Chinese State 973 projects (2014CB440801, 2007CB411307), and Hong Kong RGC (7066/07P). This paper is a contribution to IGCP 592.

## References

CHAI FM, ZHANG ZC, MAO JW, DONG LH, ZHANG ZH, WU H (2008) Geology, petrology and geochemistry of the

- Baishiquan Ni–Cu-bearing mafic–ultramafic intrusions in Xinjiang, NW China: implications for tectonics and genesis of ores. *J Asian Earth Sci* 32: 218–235
- CHEN SP, WANG DH, QU WJ, CHEN ZH, GAO XL (2005) Geological features and ore formation of the Hulu Cu–Ni sulfide deposits, Eastern Tianshan. *Xinjiang Geol* 23: 230–233 (in Chinese with English abstract)
- CHUNG SL, WANG KL, CRAWFORD AJ, KAMENETSKY VS, CHEN CH, LAN CY, CHEN CH (2001) High-Mg potassic rocks from Taiwan: implications for the genesis of orogenic potassic lavas. *Lithos* 59: 153–170
- CLASS C, MILLER DM, GOLDSTEIN SL, LANGMUIR CH (2000) Distinguishing melt and fluid subduction components in Umnak Volcanics, Aleutian Arc. *Geochem Geophys Geosyst* 2: DOI: 10.1029/1999GC000010
- COLEMAN R (1989) Continental growth of northwest China. *Tectonics* 8: 621–635
- DE HOLLANDA MHBM, PIMENTEL MM, DE SÁ EFJ (2003) Paleoproterozoic subduction-related metasomatic signatures in the lithospheric mantle beneath NE Brazil: inferences from trace element and Sr–Nd–Pb isotopic compositions of Neoproterozoic high-K igneous rocks. *J South Amer Earth Sci* 15: 885–900
- DHUIE B, BOSCH D, BODINIER JL, GARRIDO CJ, BRUGUIER O (2007) Multistage evolution of the Jijal ultramafic–mafic complex (Kohistan, N Pakistan): implications for building the roots of island arcs. *Earth Planet Sci Lett* 261: 179–200
- DU AD, WU SQ, SUN DZ, WANG SX, QU WJ, MARKEY R, STEIN H, MORGAN JW, MALINOVSKIY D (2004) Preparation and certification of Re–Os dating reference materials: molybdenite HLP and JDC. *Geost Geoanal Res* 28: 41–52
- ELLIOTT T, PLANK T, ZINDLER A, WHITE W, BOURDON B (1997) Element transport from slab to volcanic front at the Mariana arc. *J Geophys Res* 102: 14991–15019
- EYUBOGLU Y, DILEK Y, BOZKURT E, BEKTAS O, ROJAY B, SEN C (2010) Structure and geochemistry of an Alaskan-type ultramafic–mafic complex in the Eastern Pontides, NE Turkey. *Gondwana Res* 18: 230–252
- FARAHAT ES, HELMY HM (2006) Abu Hamamid Neoproterozoic Alaskan-type complex, south Eastern Desert, Egypt. *J African Earth Sci* 45: 187–197
- FOSTER G, LAMBERT DD, FRICK LR, MAAS R (1996) Re–Os isotopic evidence for genesis of Archaean nickel ores from uncontaminated komatiites. *Nature* 382: 703–706
- FRICK LR, LAMBERT DD, CARTWRIGHT I (1996) Re–Os dating of metamorphism in the Lewisian Complex, NW Scotland. *Goldschmidt Symposium 1*: 185 (Abstract)
- GAO S, LIU XM, YUAN HL, HATTENDORF B, GUNTHER D, CHEN L, HU SH (2002) Determination of forty two major and trace elements in USGS and NIST SRM glasses by laser ablation inductively coupled plasma-mass spectrometry. *Geost News* 26: 191–196
- HAN BF, JI JQ, SONG B, CHEN LH, LI ZH (2004) SHRIMP U–Pb zircon age of the mafic–ultramafic rocks and geological significance in Kalatongke and Huangshan, Xinjiang. *Chin Sci Bull* 49: 2324–2328 (in Chinese)
- HAN CM, XIAO WJ, ZHAO GC, QU WJ, DU AD (2007) Re–Os dating of the Kalatongke Cu–Ni deposit, Altay Shan, NW China, and resulting geodynamic implications. *Ore Geol Rev* 32: 452–468
- HAN CM, XIAO WJ, ZHAO GC, AO SJ, ZHANG JE, QU WJ, DU AD (2010) In-situ U–Pb, Hf and Re–Os isotopic analyses of the Xiangshan Ni–Cu–Co deposit in Eastern Tianshan (Xinjiang), Central Asia Orogenic Belt: constraints on the timing and genesis of the mineralization. *Lithos* 120: 47–562
- HAN CM, XIAO WJ, ZHAO GC, SU BX, AO SJ, ZHANG JE, WAN B (2013) Age and tectonic setting of magmatic sulfide Cu–Ni mineralization in the Eastern Tianshan Orogenic Belt, Xinjiang, Central Asia. *J Geosci* 58: 237–254
- HAURI EK, HART SR (1993) Re–Os isotope systematics of HIMU and EMII oceanic island basalts from the South Pacific Ocean. *Earth Planet Sci Lett* 114: 353–371
- HAWKESWORTH CJ, GALLAGHER K, HEROT JM, McDERMOTT F (1993) Mantle and slab contributions in arc magmas. *Ann Rev Earth Planet Sci* 21: 175–204
- HAWKESWORTH CJ, TURNER SP, McDERMOTT F, PEATE DW, CALSTEREN P (1997) U–Th isotopes in arc magmas: implications for element transfer from the subducted crust. *Science* 276: 551–555
- HIMMELBERG GR, LONEY RA (1995) Characteristics and petrogenesis of Alaskan-type ultramafic–mafic intrusions, southern Alaska. United States Government Printing Office, Washington, pp 1–41
- HOATSON DM, BLAKE DH (2000) Geology and economic potential of the Palaeoproterozoic layered mafic–ultramafic intrusions in the East Kimberley, Western Australia. *Australian Geological Survey Bulletin* 246: pp 1–469
- HOFMANN AW (1997) Mantle geochemistry: the message from oceanic volcanism. *Nature* 385: 219–229
- HU KB, YAO SZ, QU WJ, DU AD, AO SJ (2008) Re–Os isotopic analysis of the Hulu Cu–Ni sulfide deposits magmatic system, East Tianshan, Xinjiang, NW China. *Acta Petrol Sin* 24: 2359–2370 (in Chinese with English abstract)
- JAFFEY AH, FLYNN KF, GLENDENIN LE, BENTLEY WC, ESSLING AM (1971) Precision measurement of half-lives and specific activities of  $^{235}\text{U}$  and  $^{238}\text{U}$ . *Phys Rev* 4: 1889–1906
- JI JS, YANG XK, LIU, GH (2000) Distribution of the gold and copper mineralization in Chol Tagh and their deposit prediction. Chinese National 305 Project 05-04: Urumqi, Xinjiang, China, pp 1–593
- JIANG CY, CHENG SL, YE SF, XIA MZ, JIANG HB, DAI YC (2006) Litho-geochemistry and petrogenesis of Zhongposhanbei mafic rock body at Beishan region, Xinjiang. *Acta Petrol Sin* 22: 115–126 (in Chinese with English abstract)

- LAMBERT DD, FOSTER JG, FRICK L R, LI C, NALDRETT AJ (1999) Re–Os isotopic systematics of the Voisey's Bay Ni–Cu–Co magmatic ore system, Labrador, Canada. *Lithos* 47: 69–88
- LI HQ, XIE CF, CHANG HL, CAI H, ZHU JP, ZHOU S (1998) Study on Metallogenetic Chronology of Nonferrous and Precious Metallic Ore Deposits in North Xinjiang, China. Geological Publishing House, Beijing, pp 1–264 (in Chinese with English abstract)
- LI HQ, CHEN FW, MEI YP, WU H, CHENG SL, YANG JQ, DAI YC (2006) Dating of the No.1 intrusion of Pobei basic–ultrabasic rocks belt, Xinjiang, and its geological significance. *Miner Depos* 25: 463–469 (in Chinese with English abstract)
- LI QL, LI XH, LIU Y, TANG GQ, YANG JH, ZHU WG (2010) Precise U–Pb and Pb–Pb dating of Phanerozoic baddeleyite by SIMS with oxygen flooding technique. *J Anal Atom Spec* 25: 1107–1113
- LI XH, LIU Y, LI QL, GUO CH, CHAMBERLAIN KR (2009) Precise determination of Phanerozoic zircon Pb/Pb age by multi-collector SIMS without external standardization. *Geochem Geophys Geosyst* 10: doi: 10.1029/2009GC002400
- LI YC, ZHAO GC, QU WJ, PAN CZ, MAO QG, DU AD (2006) Re–Os isotopic dating of the Xiangshan deposit, East Tianshan, NW China. *Acta Petrol Sin* 22: 245–251 (in Chinese with English abstract)
- LOUCKS RR (1990) Discrimination from ophiolitic and non-ophiolitic ultramafic–mafic allochthons in orogenic belts by the Al/Ti ratios in clinopyroxene. *Geology* 18: 346–349
- LUDWIG KR (2001) User's Manual for Isoplot/Ex rev. 2.49. Berkeley Geochronology Centre Special Publications 1a: pp 1–56
- MA XX, SHU LS, SANTOSH M, LI JY (2012a) Detrital zircon U–Pb geochronology and Hf isotope data from Central Tianshan suggesting a link with the Tarim Block: implications on Proterozoic supercontinent history. *Precambr Res* 206–207: 1–16
- MA XX, SHU LS, JAHN B-M, ZHU WB, FAURE M (2012b) Precambrian tectonic evolution of Central Tianshan, NW China: constraints from U–Pb dating and in-situ Hf isotopic analysis of detrital zircons. *Precambr Res* 222–223: 450–473
- MA XX, GUO J, LIU F, QIAN Q, FAN H (2013a) Zircon U–Pb ages, trace elements and Nd–Hf isotopic geochemistry of Guyang sanukitoids and related rocks: implications for the Archean crustal evolution of the Yinshan Block, North China Craton. *Precambr Res* 230: 61–78.
- MA XX, SHU LS, SANTOSH M, LI J (2013b) Paleoproterozoic collisional orogeny in Central Tianshan: assembling the Tarim Block within the Columbia Supercontinent. *Precambr Res* 228: 1–19
- MAIER WD, BARNES SJ, CHINYEPI G, BARTON JJ, EGLINGTON B, SETSHEDI I (2008) The composition of magmatic Ni–Cu–(PGE) sulfide deposits in the Tati and Selebi–Phikwe belts of eastern Botswana. *Miner Depos* 43: 37–60
- MAO JW, YANG JM, QU WJ, DU AD, WANG Z L, HAN CM (2002) Re–Os age of Cu–Ni ores from the Huangshandong Cu–Ni sulfide deposit in the East Tianshan Mountains and its implication for geodynamic processes. *Miner Depos* 21: 323–330 (in Chinese with English abstract)
- MAO QG, XIAO WJ, HAN CM, SUN M, YUAN C, YAN Z, YONG Y, ZHANG JE (2006) Zircon U–Pb age and the geochemistry of the Baishiquan mafic–ultramafic complex in the Eastern Tianshan, Xinjiang province: constraints on the closure of the Paleo-Asian Ocean. *Acta Petrol Sin* 22: 153–162 (in Chinese with English abstract)
- MARKEY R, STEIN H, MORGAN J (1998) Highly precise Re–Os dating for molybdenite using alkaline fusion and NTIMS. *Talanta* 45: 935–946
- MARTIN CE (1991) Osmium isotopic characteristics of mantle-derived rocks. *Geochim Cosmochim Acta* 55: 1421–1434
- MCDONOUGH WF, SUN SS (1995) The composition of the Earth. *Chem Geol* 120: 223–253
- MEISEL T, WALKER RJ, MORGAN JW (1996) The osmium isotopic composition of the Earth's primitive upper mantle. *Nature* 383: 517–520
- NALDRETT AJ (1999) World-class Ni–Cu–(PGE) sulfide deposits: key factors in their genesis. *Miner Depos* 34: 227–240
- NALDRETT AJ (2004) *Magmatic Sulfide Deposits: Geology, Geochemistry and Exploration*. Springer Verlag, Heidelberg, pp 1–728
- NALDRETT AJ (2010) From the mantle to the bank: the life of a Ni–Cu–(PGE) sulfide deposit. *South African J Geol* 113: 1–32
- PEARCE JA (1996) A user's guide to basalt discrimination diagrams. In: WYMAN DA (ed) *Trace Element Geochemistry of Volcanic Rocks: Applications For Massive Sulphide Exploration*. Geological Association of Canada, Short Course Notes 12: pp 79–113
- PELTONEN P (1995) Petrogenesis of ultramafic rocks in the Vammala Nickel Belt: implication for crustal evolution of the early Proterozoic Svecofennian arc terrane. *Lithos* 34: 253–274
- PINA R, LUNAR R, ORTEGA L, GERVILLA F, ALAPIETI T, MARTINEZ C (2006) Petrology and geochemistry of mafic–ultramafic fragments from the Aguablanca Ni–Cu ore breccia, southwest Spain. *Econ Geol* 101: 865–881
- PLANK T, LANGMUIR CH (1992) Sediments melt and basaltic crust dehydrates at subduction zones. *EOS, Transactions American Geophysical Union* 73: 637
- QIN KZ, SUN S, LI JL, FANG TH, WANG SL, LIU W (2002) Paleozoic epithermal Au and porphyry Cu Deposits in North Xinjiang, China: epochs, features, tectonic linkage and exploration significance. *Res Geol* 52: 291–300

- QIN KZ, ZHANG LC, XIAO WJ, XU XW, YAN Z, MAO JW (2003) Overview of major Au, Cu, Ni and Fe deposits and metallogenic evolution of the eastern Tianshan Mountains, northwestern China. In: MAO JW, GOLDFARB RJ, SELTMANN R, WANG DH, XIAO WJ, HART C (eds) *Tectonic Evolution and Metallogeny of the Chinese Altay and Tianshan*. IAGOD Guidebook Series 10: 227–249
- RAVIZZA G, TUREKIAN KK, HAY BJ (1991) The geochemistry of rhenium and osmium in recent sediments from the Black Sea. *Geochim Cosmochim Acta* 55: 3741–3752
- RIPLEY EM, LAMBERT DD, FRICK LR (1998) Re–Os, Sm–Nd, and Pb isotopic constraints on mantle and crustal contributions to magmatic sulfide mineralization in the Duluth Complex. *Geochim Cosmochim Acta* 62: 3349–3365
- SEGHEDI I, DOWNES H, VASELLI O, SZAKÁCS A, BALOGH K, PÉCSKAY Z (2004) Post-collisional Tertiary–Quaternary mafic alkalic magmatism in the Carpathian–Pannonian region: a review. *Tectonophysics* 393: 43–62
- SCHOENE B, CROWLEY JL, CONDON DJ, SCHMITZ MD, BOWRING SA (2006) Reassessing the uranium decay constants for geochronology using ID-TIMS U/Pb data. *Geochim Cosmochim Acta* 70: 426–445
- SHIREY SB, WALKER RJ (1998) The Re–Os isotope system in cosmochemistry and high-temperature geochemistry. *Ann Rev Earth Planet Sci* 26: 423–500
- SHU L, CHARVET J, LU H, LAURENT-CHARVET S (2002) Paleozoic accretion–collision events and kinematics of deformation in the eastern part of the Southern–Central Tianshan Belt, China. *Acta Geol Sin* 76: 308–323
- SMOLIAR ML, WALKER RJ, MORGAN JW (1996) Re–Os ages of group IIA, IIIA, IVA and VIB iron meteorites. *Science* 271: 1099–1102
- SNOW JE, REISBERG L (1995) Os isotope systematics of the MORB mantle: results from altered abyssal peridotites. *Earth Planet Sci Lett* 133: 411–421
- STACEY JS, KRAMERS JD (1975) Approximation of terrestrial lead isotope evolution by a two-stage model. *Earth Planet Sci Lett* 26: 207–221
- STEIN HJ, SUNDBLAD K, MARKEY RJ, MORGAN MJ (1998) Re–Os ages for Archean molybdenite and pyrite, Kuitila–Kivisuo, Finland, and Proterozoic molybdenite, Lithuania: testing the chronometer in a metamorphic and metasomatic setting. *Miner Depos* 33: 329–345
- STOLZ AJ, JOCHUM KP, HOFMANN AW (1996) Fluid- and melt-related enrichment in the subarc mantle; evidence from Nb/Ta variations in island-arc basalts. *Geology* 24: 587–590
- SUN H (2009) Ore-forming mechanism in conduit system and ore-bearing property evaluation for mafic-ultramafic complex in Eastern Tianshan, Xinjiang. Unpublished PhD thesis, Institute of Geology and Geophysics, Chinese Academy of Sciences, Beijing, pp 1–274 (in Chinese with English abstract)
- SUN H, QIN KZ, LI JX, TANG DM, FAN X, XIAO QH (2008) Constraint of mantle partial melting on PGE mineralization of mafic–ultramafic intrusions in Eastern Tianshan: case study on Tulargen and Xiangshan Cu–Ni deposits. *Acta Petrol Sin* 24: 1079–1086
- SUN SS, MCDONOUGH WF (1989) Chemical and isotopic systematics of oceanic basalts: implications for mantle composition and processes. In: SAUNDERS AD, NORRIS MJ (eds) *Magmatism in the Ocean Basins*. Geological Society London Special Publications 42: pp 313–345
- TANG DM (2009) Geochemical tracing and enrichment regularity of platinum-group element (PGE) in nickel–copper sulfide deposits hosted in post-collision mafic–ultramafic intrusions, Eastern Tianshan. Unpublished PhD thesis, Institute of Geology and Geophysics, Chinese Academy of Sciences, Beijing, pp 1–204 (in Chinese with English abstract)
- TAYLOR SR, MCLENNAN SM (1985) *The Continental Crust: Its Composition and Evolution*. Blackwell Scientific Publications, London, pp 1–312
- THAKURTA J, RIPLEY EM, LI C (2008) Geochemical constraints on the origin of sulfide mineralization in the Duke Island Complex, southeastern Alaska. *Geochem Geophys Geosyst* 9: doi: 10.1029/2008GC001982
- TURNER S, HAWKESWORTH CJ, CALSTEREN P, HEATH E, MACDONALD R, BLACK S (1996) U-series isotopes and destructive plate margin magma genesis in the Lesser Antilles. *Earth Planet Sci Lett* 142: 191–207
- WALKER RJ, MORGAN JW (1989) Rhenium–osmium isotope systematics of carbonaceous chondrites. *Science* 243: 519–522
- WALKER RJ, SHIREY SB, STECHER O (1988) Comparative Re–Os, Sm–Nd and Rb–Sr isotope and trace element systematics for Archean komatiites flows from Munro Township, Abitibi Belt, Ontario. *Earth Planet Sci Lett* 87: 1–12
- WALKER RJ, CARLSON RW, SHIREY SB, BOYD FR (1989) Os, Sr, Nd and Pb isotope systematics of southern African peridotite xenoliths: implications for the chemical evolution of subcontinental mantle. *Geochim Cosmochim Acta* 53: 1583–1595
- WALKER RJ, MORGAN JW, NALDRETT AJ, LI C, FASSETT JD (1991) Re–Os isotope systematics of Ni–Cu sulfide ores, Sudbury igneous complex, Ontario: Evidence for a major crustal component. *Earth Planet Sci Lett* 105: 416–429
- WALKER RJ, MORGAN JW, HORAN MF, CZAMANSKE GK, KROGSTAD EJ, FEDORENKO VA, KUNILOV VE (1994) Re–Os isotopic evidence for an enriched-mantle source for the Noril’sk-type, ore-bearing intrusions, Siberia. *Geochim Cosmochim Acta* 58: 4179–4197
- WANG H, QU WJ, LI HQ, CHEN SP (2007) Dating and discussion on the rock-forming and ore-forming age of newly-discovered Cu–Ni-sulfide deposits in Hami, Xinjiang. *Acta Geol Sin* 81: 526–529 (in Chinese with English abstract)

- WANG RM, LI SC (1987) Physical-chemical condition of diagenetic and ore-forming of Huangshandong Cu–Ni sulphide deposit, Hami, Xinjiang. *J Chengdu College Geol* 14: 1–9 (in Chinese)
- WANG YW, WANG JB, WANG LJ, PENG XM, HUI WD, QIN QX (2006) A intermediate type of Cu–Ni sulfide and V–Ti magnetite deposit: Xiangshan deposit, Hami, Xinjiang, China. *Acta Geol Sin* 80: 61–73
- WIEDENBECK M, ALLÉ P, CORFU F, GRIFFIN WL, MEIER M, OBERLI F, VON QUADT A, RODDICK JC, SPIEGEL W (1995) Three natural zircon standards for U–Th–Pb, Lu–Hf, trace-element and REE analyses. *Geost News* 19: 1–23
- WILHEM C, WINDLEY BF, STAMPFLI GM (2012) The Altaids of Central Asia: a tectonic and evolutionary innovative review. *Earth Sci Rev* 113: 303–341
- WU YB, ZHENG YF (2004) Genesis of zircon and its constraints on interpretation of U–Pb age. *Chin Sci Bull* 49: 1554–1569
- WU H, LI HQ, MO XH, CHEN FW, LU YF, MEI YP, DENG G (2005) Age of the Baishiquan mafic–ultramafic complex, Hami, Xinjiang and its geological significance. *Acta Geol Sin* 79: 498–502 (in Chinese with English abstract)
- XIAO WJ, WINDLEY BF, BADARCH G, SUN S, LI J, QIN K, WANG Z (2004a) Palaeozoic accretionary and convergent tectonics of the southern Altaids: implications for the growth of Central Asia. *J Geol Soc, London* 161: 339–342
- XIAO WJ, ZHANG LC, QIN KZ, SUN S, LI JL (2004b) Paleozoic accretionary and collisional tectonics of the Eastern Tianshan (China): implications for the continental growth of central Asia. *Amer J Sci* 304: 370–395
- XU ZQ, HE BZ, ZHANG CL, ZHANG JX, WANG ZM, CAI ZH (2013) Tectonic framework and crustal evolution of the Precambrian basement of the Tarim Block in NW China: new geochronological evidence from deep drilling samples. *Precambr Res* 235: 150–162
- YANG XK, TAO HX, LUO GC, JI JS (1996) Basic features of plate tectonics in Eastern Tianshan of China. *Xinjiang Geol* 14: 221–227
- YANG XK, CHENG HB, JI JS, LUO GC, TAO HX (2000) Analysis on gold and copper ore-forming setting with ore-forming system of Eastern Tianshan. *J Xi'an Engineering Univ* 22: 7–14
- ZHANG ZH, CHAI FM, DU AD, ZHANG ZC, YAN SH, YANG JM, QU WJ, WANG ZL (2005) Re–Os dating and trace on the ore-forming materials for Cu–Ni sulfide ores of the Karatungk deposit in northern Xinjiang. *Acta Petrol Miner* 24: 285–293 (in Chinese with English abstract)
- ZHANG ZH, WANG ZL, WANG YB, ZUO GC, WANG LS (2007) SHRIMP zircon U–Pb dating of diorite from Qingbulake basic complex in western Tianshan Mountains of Xinjiang and its geological significance. *Miner Depos* 26: 353–360 (in Chinese with English abstract)
- ZHAO JH, ZHOU MF (2007) Geochemistry of Neoproterozoic mafic intrusions in the Panzhihua district (Sichuan Province, SW China): implications for subduction related metasomatism in the upper mantle. *Precambr Res* 152: 27–47
- ZHENG YF, XIAO WJ, ZHAO GC (2013) Introduction to tectonics of China. *Gondwana Res* 23: 1189–1206
- ZHOU JY, CUI BF, XIAO HL, CHEN SZ, ZHU DM (2001) The Kangguertag–Huangshan collision zone of bilateral subduction and its metallogenic model and prognosis in Xinjiang, China. *Volcanol Mineral Resour* 22: 252–263
- ZHOU MF, LESHNER CM, YANG ZX, LI JW, SUN M (2004) Geochemistry and petrogenesis of 270 Ma Ni–Cu–(PGE) sulfide-bearing mafic intrusions in the Huangshan district, eastern Xinjiang, northwestern China: implication for the tectonic evolution of the Central Asian Orogenic Belt. *Chem Geol* 209: 233–257
- ZOU HB, ZINDLER A, XU XS, QI U (2000) Major, trace element, and Nd, Sr and Pb isotope studies of Cenozoic basalts in SE China: mantle sources, regional variations, and tectonic significance. *Chem Geol* 171: 33–47